ENTATION PAGE

Form Approved
OMB No 0704-0188

1. AGENCY USE ONLY (Leave blank)	2. REPORT DATE	3. REPORT TYPE AND DATES COVERED
	20-OCT-1992	

4. TITLE AND SUBTITLE
Progress in Developing a Transition Model for High-Speed Flows

5. FUNDING NUMBERS

6. AUTHOR(S)
David C. Wilcox

7. PERFORMING ORGANIZATION NAME(S) AND ADDRESS(ES)
DCW Industries, Inc.
5354 Palm Drive
La Canada, California 91011

8. PERFORMING ORGANIZATION REPORT NUMBER

9. SPONSORING / MONITORING AGENCY NAME(S) AND ADDRESS(ES)
U. S. Army Research Office
P. O. Box 12211
Research Triangle Park, NC 27709-2211

10. SPONSORING / MONITORING AGENCY REPORT NUMBER
ARO 26863.7-EG-S

11. SUPPLEMENTARY NOTES
The view, opinions and/or findings contained in this report are those of the author(s) and should not be construed as an official Department of the Army position, policy, or decision, unless so designated by other documentation.

12a. DISTRIBUTION / AVAILABILITY STATEMENT
Approved for public release; distribution unlimited.

12b. DISTRIBUTION CODE

13. ABSTRACT *(Maximum 200 words)*

This report summarizes research conducted during the past year whose aim is to develop and test an accurate and efficient method for describing boundary-layer development in the transition region. A low-Reynolds-number version of the Wilcox k-ω model has been postulated and tested against experimental data for 10 fully turbulent boundary layers and for more than 20 transitional cases. Overall discrepancies between theory and experiment are smaller than those for simpler correlations designed for use with algebraic turbulence models. Singular perturbation analysis of the compressible viscous sublayer and defect layer has been initiated with some interesting preliminary results. Some progress has been made toward eliminating the k-ω model's sensitivity to the freestream boundary condition on ω.

14. SUBJECT TERMS
TRANSITION, TURBULENCE MODELING, HYPERSONICS, COMPUTATIONAL FLUID DYNAMICS

15. NUMBER OF PAGES
46

16. PRICE CODE

17. SECURITY CLASSIFICATION OF REPORT	18. SECURITY CLASSIFICATION OF THIS PAGE	19. SECURITY CLASSIFICATION OF ABSTRACT	20. LIMITATION OF ABSTRACT
UNCLASSIFIED	UNCLASSIFIED	UNCLASSIFIED	UL

Contents

Abstract

This report summarizes research conducted during the past year whose aim is to develop and test an accurate and efficient method for describing boundary-layer development in the transition region. A low-Reynolds-number version of the Wilcox $k-\omega$ model has been postulated and tested against experimental data for 10 fully turbulent boundary layers and for more than 20 transitional cases. Overall discrepancies between theory and experiment are smaller than those for simpler correlations designed for use with algebraic turbulence models. Singular perturbation analysis of the compressible viscous sublayer and defect layer has been initiated with some interesting preliminary results. Some progress has been made toward eliminating the $k-\omega$ model's sensitivity to the freestream boundary condition on ω.

Chapter 1

Introduction

The purpose of this research project for the past three years has been to develop analytical and computational tools suitable for predicting properties of hypersonic turbulent flows. Significant progress has been made on several aspects of the turbulent-flow problem, especially in representing low-Reynolds-number effects and boundary-layer transition. Because of the importance of transition in hypersonic boundary layers, most of our research during the past year has focused exclusively the transition problem.

The overall objective of our approach to the transition problem is to use the Wilcox[1] $k-\omega$ turbulence model as the foundation for studying and modeling the transitional flow region. Consistent with the needs of NASA, the transition point is assumed to be known a priori. Computations can thus be initiated at the known transition location and continued downstream through the transitional flow region and well into the fully turbulent region. To develop the model, we have followed a sequence of interrelated steps.

1. We have drawn from the extensive work done by Wilcox[2-7] to help formulate a low-Reynolds-number version of the $k-\omega$ model. While much of this early research focused on locating the transition point, some of the analysis (most notably Wilcox[6]) revealed the way in which the model equations describe the growth of the instability from the transition point to the fully turbulent regime.

2. We have simulated several of the flows that have been done with Direct Numerical Simulation (DNS) methods. The results of Mansour, Kim and Moin[8] have received immediate attention for two different Reynolds numbers. Comparing model predictions with the DNS results helped greatly in developing the model.

3. We have tested the model against 10 two-dimensional, fully turbulent boundary layers, including both incompressible and compressible cases.

4. We have tested the model against all of the two-dimensional cases presented by Singer, Dinavahi, and Iyer.[3]

5. We have done some analysis specifically aimed at eliminating the $k-\omega$ model's sensitivity to the freestream boundary condition on ω.

6. We have initiated a singular perturbation analysis of the compressible turbulent boundary layer to help quantify effects of compressibility on model predictions.

Addressing Items 1 and 2 has produced a low-Reynolds-number version of the $k-\omega$ model. Wilcox[10] describes the model and presents applications to fully turbulent channel and pipe flow, and for a transitional, incompressible flat-plate boundary layer. He also clarifies the manner in which the model predicts transition.

This report applies the model to 10 turbulent boundary-layer test cases and to more than 20 transitional flows for which experimental data are available. The applications show that additional model development is needed to properly account for effects of compressibility. We have initiated the new model development efforts by addressing Items 4 and 5.

Chapter 2 summarizes the low-Reynolds-number version of the $k-\omega$ model. Chapters 3 and 4 present results of our applications. Boundary condition and closure coefficient sensitivity is discussed in Chapter 5. We analyze the compressible turbulent boundary layer in Chapter 6. Chapter 7 summarizes results of the research.

Chapter 2

Low-Reynolds-Number k–ω Model

The equations of motion for the Wilcox[10] low-Reynolds-number $k-\omega$ model were initially postulated for incompressible flows. To generalize for compressible flows, we introduce Favre[11] mass averaged variables and rewrite the equations of motion as follows.

$$\frac{\partial \rho}{\partial t} + \frac{\partial}{\partial x_j}(\rho u_j) = 0 \tag{2.1}$$

$$\frac{\partial}{\partial t}(\rho u_i) + \frac{\partial}{\partial x_j}(\rho u_j u_i) = -\frac{\partial p}{\partial x_i} + \frac{\partial \tau_{ji}}{\partial x_j} \tag{2.2}$$

$$\frac{\partial}{\partial t}(\rho E) + \frac{\partial}{\partial x_j}(\rho u_j H) = \frac{\partial}{\partial x_j}\left[u_i \tau_{ij} - q_j + (\mu + \sigma^* \mu_T)\frac{\partial k}{\partial x_j}\right] \tag{2.3}$$

$$\frac{\partial}{\partial t}(\rho k) + \frac{\partial}{\partial x_j}(\rho u_j k) = \tau_{ij}^T \frac{\partial u_i}{\partial x_j} - \beta^* \rho \omega k + \frac{\partial}{\partial x_j}\left[(\mu + \sigma^* \mu_T)\frac{\partial k}{\partial x_j}\right] \tag{2.4}$$

$$\frac{\partial}{\partial t}(\rho \omega) + \frac{\partial}{\partial x_j}(\rho u_j \omega) = \alpha \frac{\omega}{k} \tau_{ij}^T \frac{\partial u_i}{\partial x_j} - \beta \rho \omega^2 + \frac{\partial}{\partial x_j}\left[(\mu + \sigma \mu_T)\frac{\partial \omega}{\partial x_j}\right] \tag{2.5}$$

In Equations (2.1)-(2.5), t and x_i denote time and position vector; ρ and p are density and pressure; u_i is mass-averaged velocity vector; E and H are total energy and total enthalpy; τ_{ij} and q_i are the total stress tensor and the total heat flux vector; τ_{ij}^T is the Reynolds stress tensor; k and ω are turbulence kinetic

energy and specific dissipation rate; and, α, β, β^*, σ, σ^* are closure coefficients. The following constitutive relations are needed to close the system.

$$\mu_T = \alpha^* \frac{\rho k}{\omega}, \qquad \tau_{ij} = \tau_{ij}^L + \tau_{ij}^T \tag{2.6}$$

$$\tau_{ij}^L = 2\mu \left(S_{ij} - \frac{1}{3} \frac{\partial u_k}{\partial x_k} \delta_{ij} \right) \tag{2.7}$$

$$\tau_{ij}^T = 2\mu_T \left(S_{ij} - \frac{1}{3} \frac{\partial u_k}{\partial x_k} \delta_{ij} \right) - \frac{2}{3} \rho k \delta_{ij} \tag{2.8}$$

$$q_j = - \left(\frac{\mu}{Pr_L} + \frac{\mu_T}{Pr_T} \right) \frac{\partial h}{\partial x_j} \tag{2.9}$$

$$E = e + \frac{1}{2} u_i u_i + k, \qquad H = h + \frac{1}{2} u_i u_i + k \tag{2.10}$$

$$S_{ij} = \frac{1}{2} \left(\frac{\partial u_i}{\partial x_j} + \frac{\partial u_j}{\partial x_i} \right) \tag{2.11}$$

In the constitutive relations, we have introduced the molecular stress tensor, τ_{ij}^L, mean strain-rate tensor, S_{ij}, molecular viscosity, μ, eddy viscosity, μ_T, enthalpy, h, laminar Prandtl number, Pr_L, turbulent Prandtl number, Pr_T, internal energy, e, and an additional closure coefficient, α^*. Finally, to complete closure of the system, we specify the values of the closure coefficients as follows.

$$\alpha^* = \frac{\alpha_o^* + Re_T/R_k}{1 + Re_T/R_k}, \qquad \alpha = \frac{5}{9} \cdot \frac{\alpha_o + Re_T/R_\omega}{1 + Re_T/R_\omega} \cdot (\alpha^*)^{-1} \tag{2.12}$$

$$\beta^* = \frac{9}{100} \cdot \frac{5/18 + (Re_T/R_\beta)^4}{1 + (Re_T/R_\beta)^4} \tag{2.13}$$

$$\beta = \frac{3}{40}, \qquad \sigma^* = \frac{1}{2}, \qquad \sigma = \frac{1}{2} \tag{2.14}$$

$$\alpha_o^* = \beta/3, \qquad \alpha_o = 1/10 \tag{2.15}$$

$$R_\beta = 6, \qquad R_k = 8, \qquad R_\omega = 27/10 \tag{2.16}$$

The quantity Re_T is the turbulence Reynolds number defined by

$$Re_T = \frac{\rho k}{\omega \mu} \tag{2.17}$$

Chapter 3

Turbulent Boundary-Layer Applications

The primary objective of this research project is to describe boundary-layer development through transition from laminar to turbulent flow. As part of this objective, it is important that we provide an accurate description in the turbulent region immediately following transition, i.e., we insist that our model approach the proper limiting state of the boundary layer. Consequently, since the $k-\omega$ model without viscous corrections generally is very accurate for turbulent boundary layers, a round of tests is in order to make sure model predictions are not adversely affected by the viscous corrections. We have performed ten boundary layer computations including effects of adverse and favorable pressure gradient, and for Mach numbers as high as 10. Table 3.1 lists the ten cases.

Table 3.1: Turbulent Boundary Layer Test Cases

Description	∇p	Data Source
Incompressible Flat Plate	None	Wieghardt-Tillman[12]
Flow 1100	Adverse	Ludweig-Tillman[13]
Flow 1200	Adverse	Ludweig-Tillman[13]
Flow 1300	Favorable	Ludweig-Tillman[13]
Bradshaw Flow C	Adverse	Bradshaw[14]
Samuel-Joubert	Adverse	Samuel-Joubert[15]
Mach 2.244 Flat Plate	None	Shutts[16]
Mach 4.544 Flat Plate	None	Coles[16]
Mach 10.31 Flat Plate	None	Watson[16]
Mach 2.653 Boundary Layer	Adverse	Fernando-Smits[17]

Incompressible Flat Plate. Figure 3.1 compares computed and measured skin friction, c_f, and sublayer-scaled velocity, u^+. As shown, the only significant difference between predictions with and without viscous corrections is in the transition point. The unmodified model undergoes transition much earlier than the model with viscous corrections. Skin friction at the final station is $2.50 \cdot 10^{-3}$ with viscous modifications compared to $2.49 \cdot 10^{-3}$ without.

Flows 1100 and 1200. Figures 3.2 and 3.3 compare computed and measured[13] c_f and u^+ for two incompressible boundary layers with adverse pressure gradient. Flow 1100 has a mild adverse gradient while Flow 1200 has a fairly strong adverse gradient. Note that computations have been terminated at the last data station upstream of $x = 3$ m. for both flows. As noted by Coles and Hirst,[19] the data fail to satisfy the momentum integral equation downstream of $x = 3$ m. and are thus unreliable. As with the flat plate case, differences between results obtained with and without viscous corrections are barely noticeable. For Flow 1100, skin friction at the final station is $1.90 \cdot 10^{-3}$ with viscous corrections and $1.93 \cdot 10^{-3}$ without. A slightly larger difference is found for Flow 1200, namely, $c_f = 1.58 \cdot 10^{-3}$ with viscous corrections and $1.61 \cdot 10^{-3}$ without.

Flow 1300. Figure 3.4 compares computed and measured properties for Flow 1300, another one of the incompressible Ludweig-Tillman[13] flows, this time with favorable pressure gradient. Velocity profile differences are noticeable only below $y^+ = 200$, and skin friction is nearly identical. Skin friction at the final station is $3.34 \cdot 10^{-3}$ with viscous corrections included and $3.35 \cdot 10^{-3}$ when they are excluded.

Bradshaw Flow C. This incompressible adverse pressure gradient case was one of the most difficult-to-predict case in Stanford Olympics I.[19] As shown in Figure 3.5, with or without viscous corrections, the $k - \omega$ model virtually duplicates measured c_f and u^+ for this flow. At the final station, $c_f = 1.60 \cdot 10^{-3}$ with viscous corrections and $1.61 \cdot 10^{-3}$ without.

Samuel-Joubert. This incompressible adverse pressure gradient boundary layer was supposed to be a simple application in Stanford Olympics II.[19] On the contrary, it proved to be very difficult for all models and has become a key test case for how well a turbulence model predicts effects of adverse pressure gradient. Figure 3.6 shows that both high- and low-Reynolds-number versions of the model nearly duplicate measured skin friction and velocity profile at the last station. At the final station, $c_f = 1.21 \cdot 10^{-3}$ with viscous corrections and $1.25 \cdot 10^{-3}$ without.

Compressible Flat Plates. As shown in Figures 3.7, 3.8 and 3.9, the viscous corrections have virtually no effect on skin friction and velocity profiles in the fully turbulent region for these three applications. For all three cases, skin friction differs by less than one percent at the final station. *This contradicts the claims of Zhang, et al*[20] *that achieving correct asymptotic near-wall behavior is required to accurately predict compressible flows.* If their claims were correct, the $k-\omega$ model: (a) would not predict flow properties so close to measurements for the Mach 2.244 and 4.544 cases; and, (b) would be closer to measurements

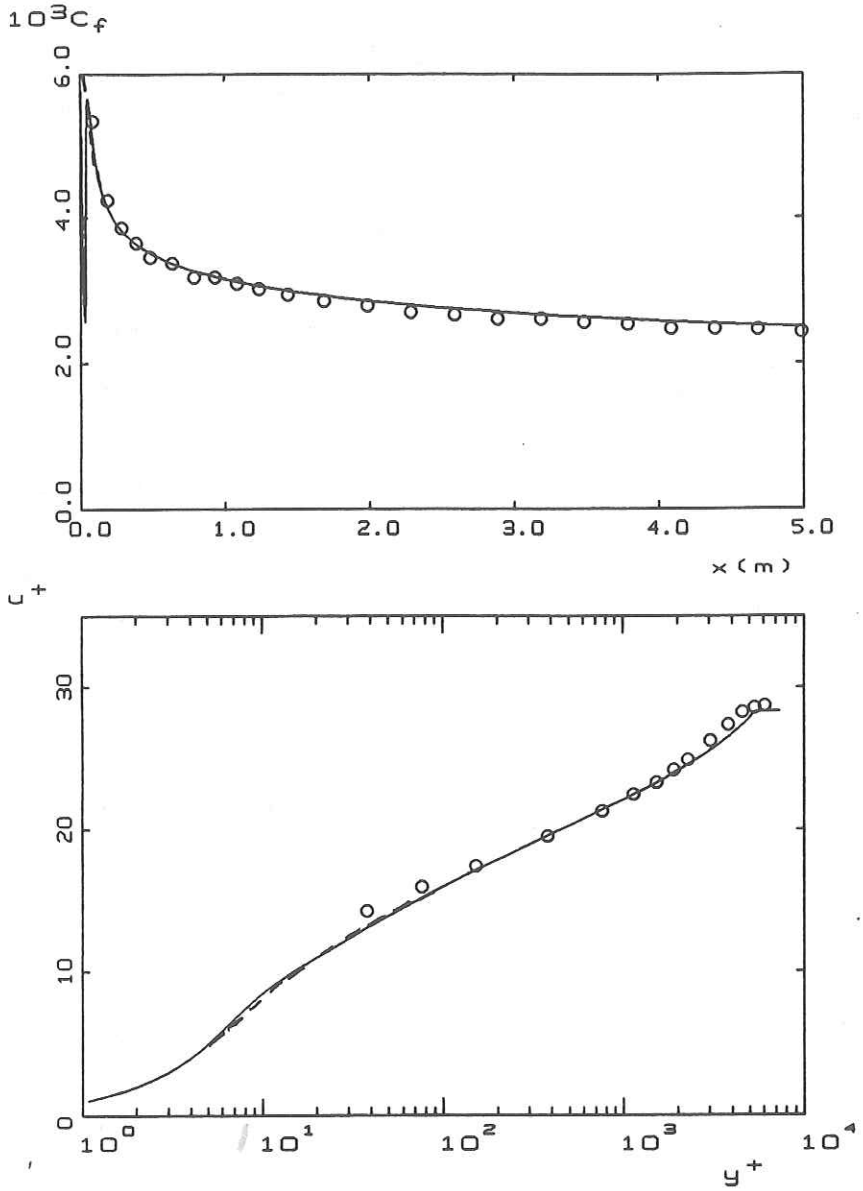

Figure 3.1: Incompressible flat-plate boundary layer; o Wieghardt-Tillman; $k-\omega$ with viscous corrections; $- - -$ $k-\omega$ without viscous corrections.

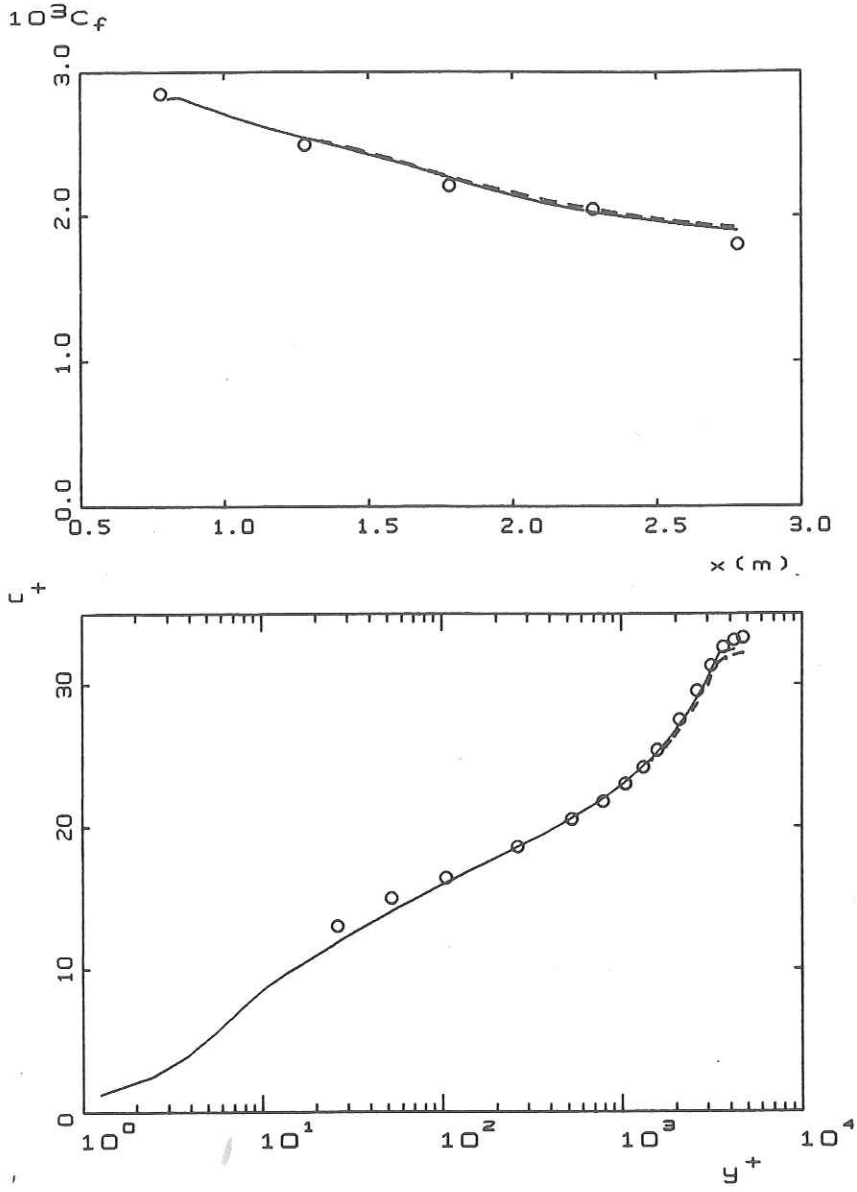

Figure 3.2: Flow 1100: Incompressible boundary layer with mild adverse pressure gradient; o Ludweig-Tillman; — $k-\omega$ with viscous corrections; – – – $k-\omega$ without viscous corrections.

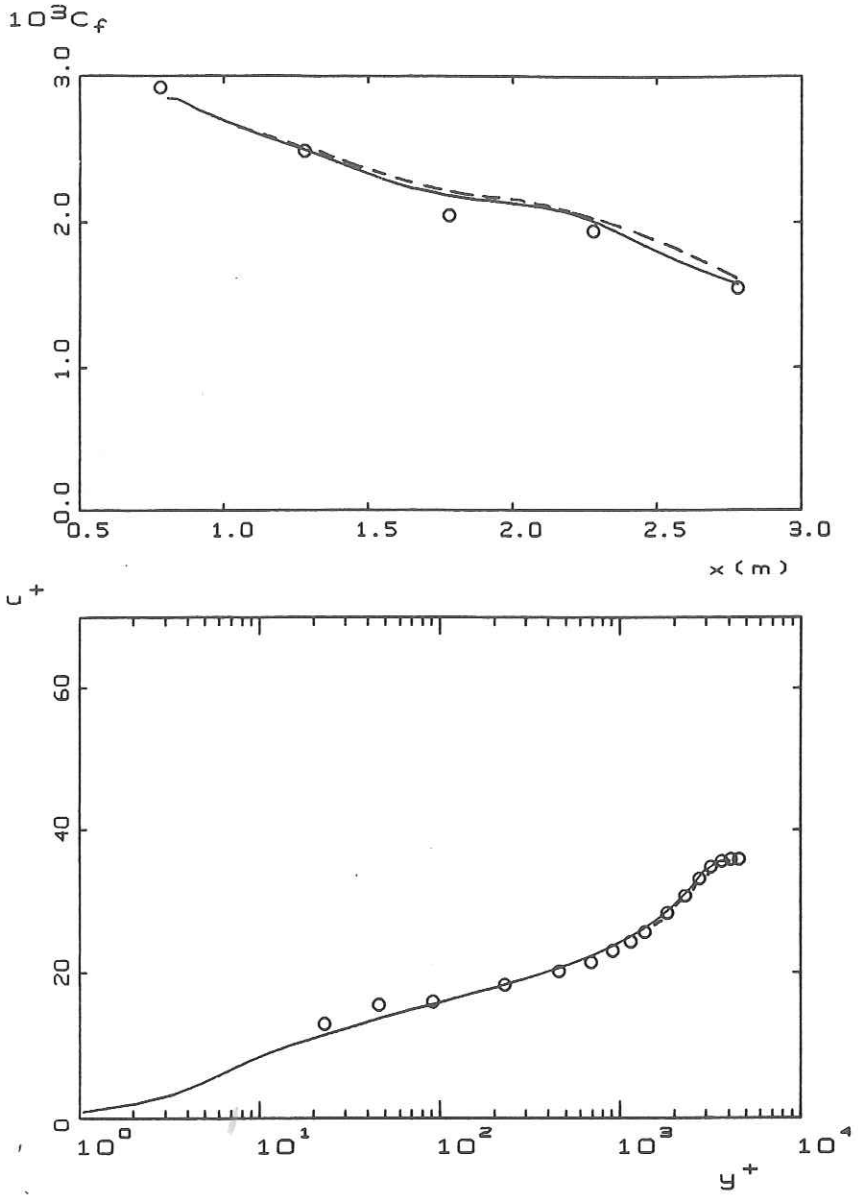

Figure 3.3: Flow 1200: Incompressible boundary layer with strong adverse pressure gradient; o Ludweig-Tillman; — $k-\omega$ with viscous corrections; – – – $k-\omega$ without viscous corrections.

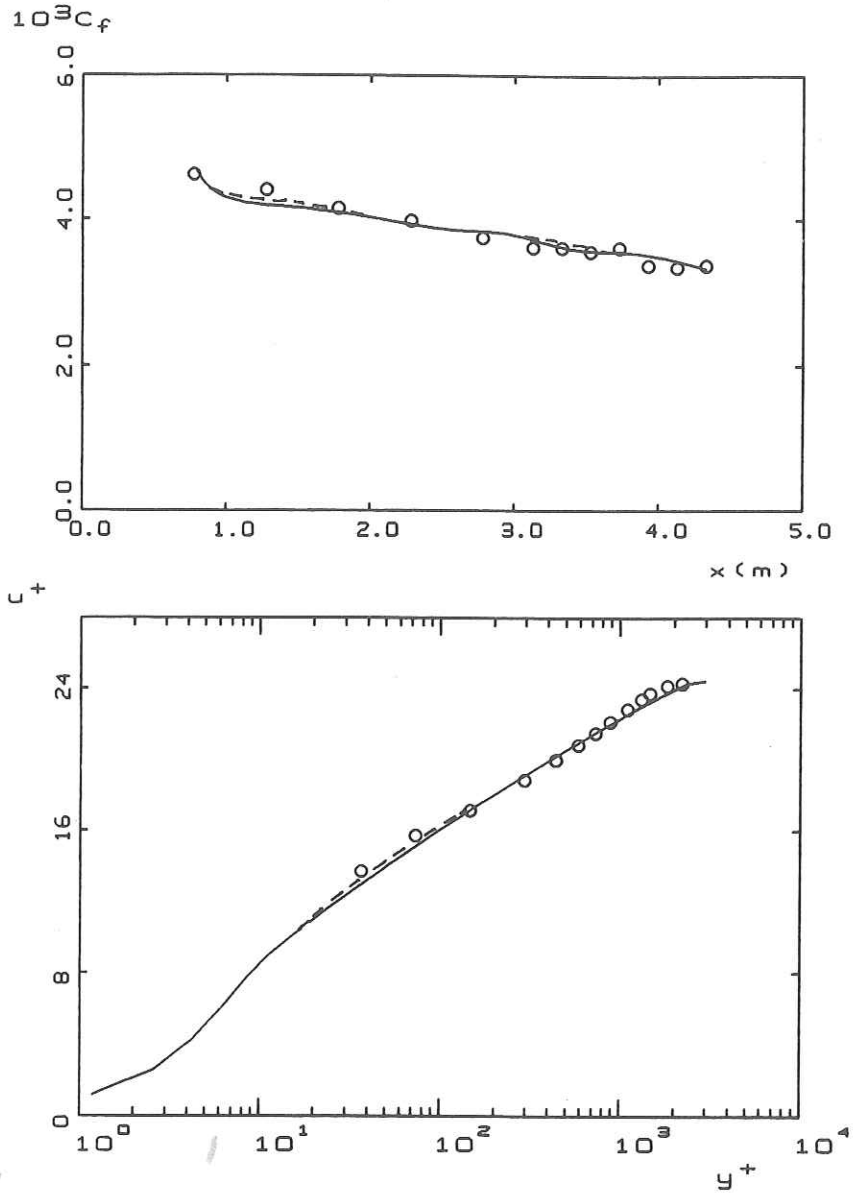

Figure 3.4: Flow 1300: Incompressible boundary layer with favorable pressure gradient; ∘ Ludweig-Tillman; — $k-\omega$ with viscous corrections; $-\ -\ -$ $k-\omega$ without viscous corrections.

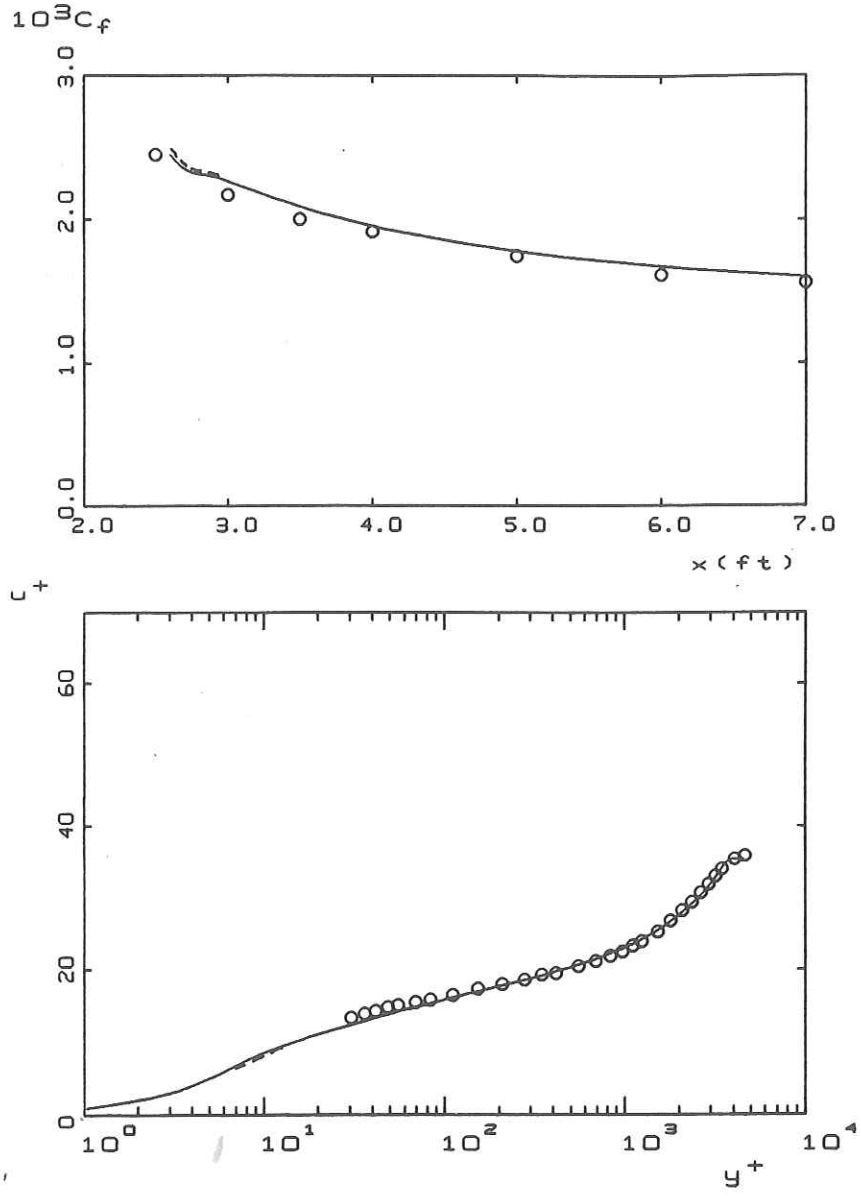

Figure 3.5: Bradshaw Flow C: Incompressible boundary layer in adverse pressure gradient; ∘ Bradshaw; — $k-\omega$ with viscous corrections; – – – $k-\omega$ without viscous corrections.

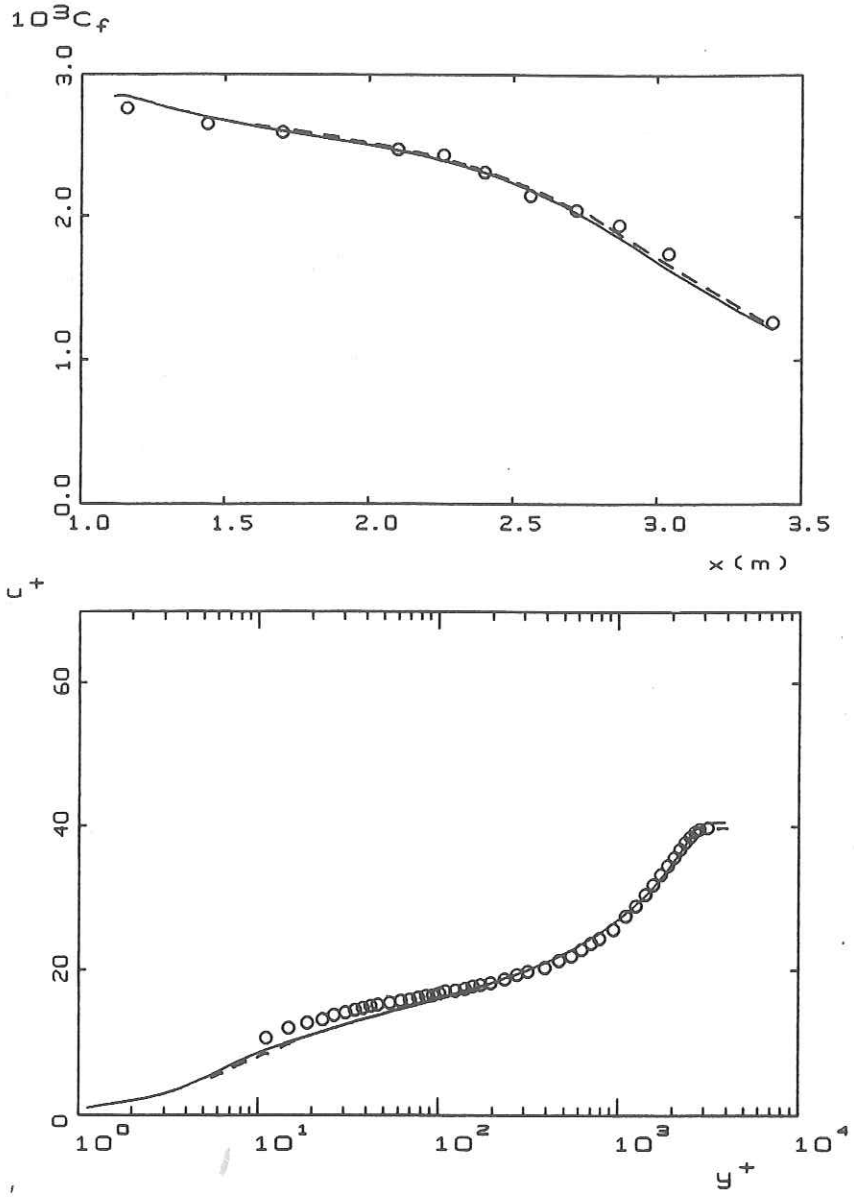

Figure 3.6: Incompressible boundary layer in an increasingly adverse pressure gradient; o Samuel-Joubert; — $k-\omega$ with viscous corrections; – – – $k-\omega$ without viscous corrections.

for the Mach 10.31 case with viscous corrections included. What their analysis actually shows that they have simply canceled the $k-\epsilon$ model's inherent flaw in defect-layer structure[1,21] by projecting their viscous modifications far above the viscous sublayer.

Mach 2.563 Boundary Layer. The final turbulent flow application is for a compressible boundary layer with a freestream Mach number of 2.563. The boundary layer is subjected to an adverse pressure gradient. Figure 3.10 shows that, as in virtually all of our applications, only slight differences are present between model predictions with and without viscous corrections. At the final station, skin friction with viscous corrections is $1.11 \cdot 10^{-3}$ and $1.10 \cdot 10^{-3}$ without.

In summary, for all ten cases considered, differences between computed flow properties with and without viscous corrections are less than 3%, and are generally less than 1%. Hence, the viscous corrections leave the best features of the $k-\omega$ model intact, i.e., the model still accurately predicts effects of pressure gradient and compressibility up to Mach 5.

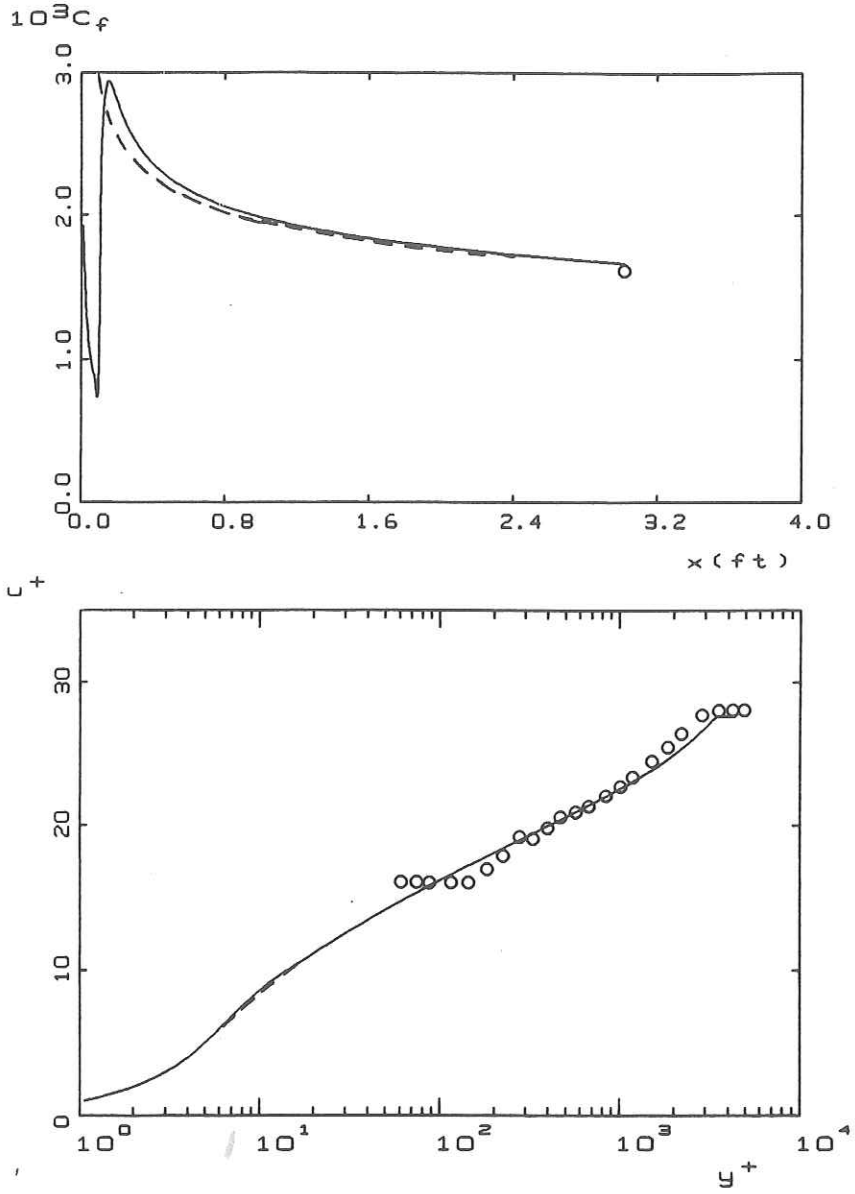

Figure 3.7: Mach 2.244 adiabatic-wall flat-plate boundary layer; ∘ Shutts; — $k-\omega$ with viscous corrections; – – – $k-\omega$ without viscous corrections.

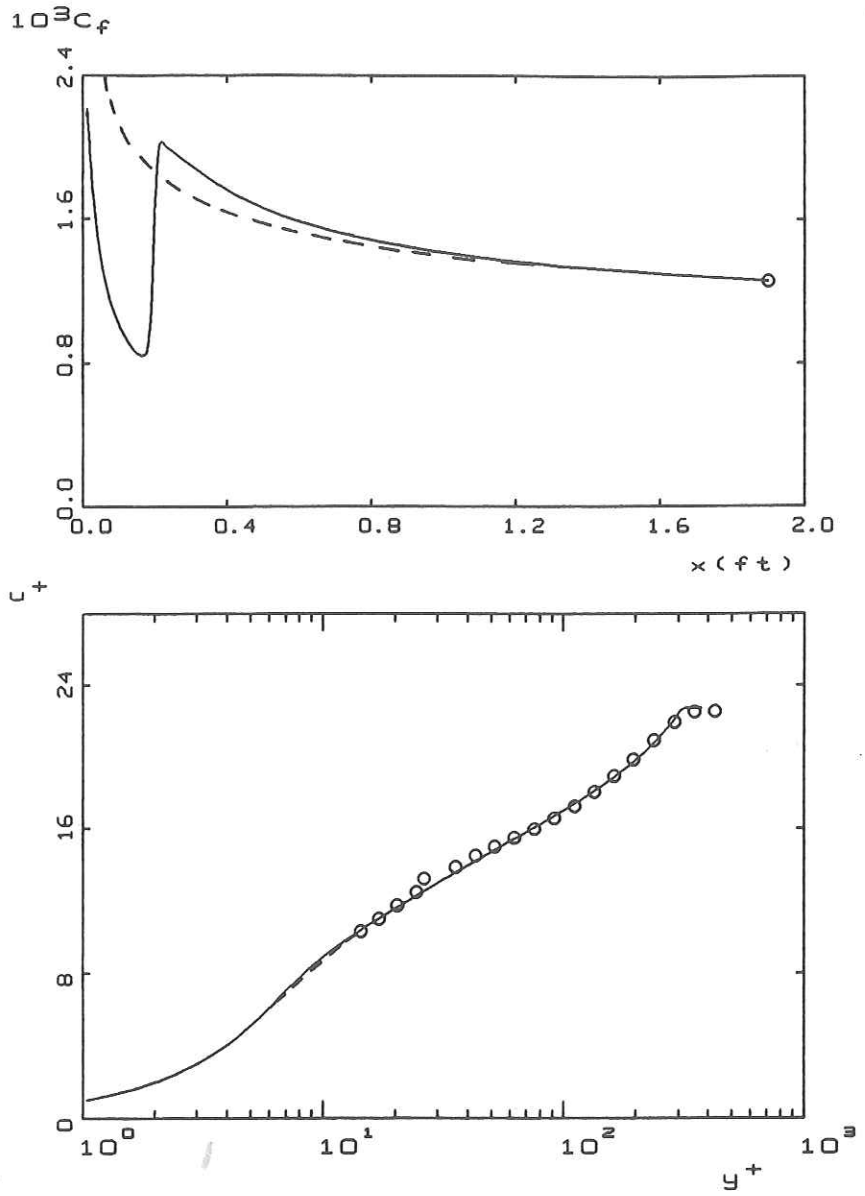

Figure 3.8: Mach 4.544 adiabatic-wall flat-plate boundary layer; o Coles; — $k-\omega$ with viscous corrections; – – – $k-\omega$ without viscous corrections.

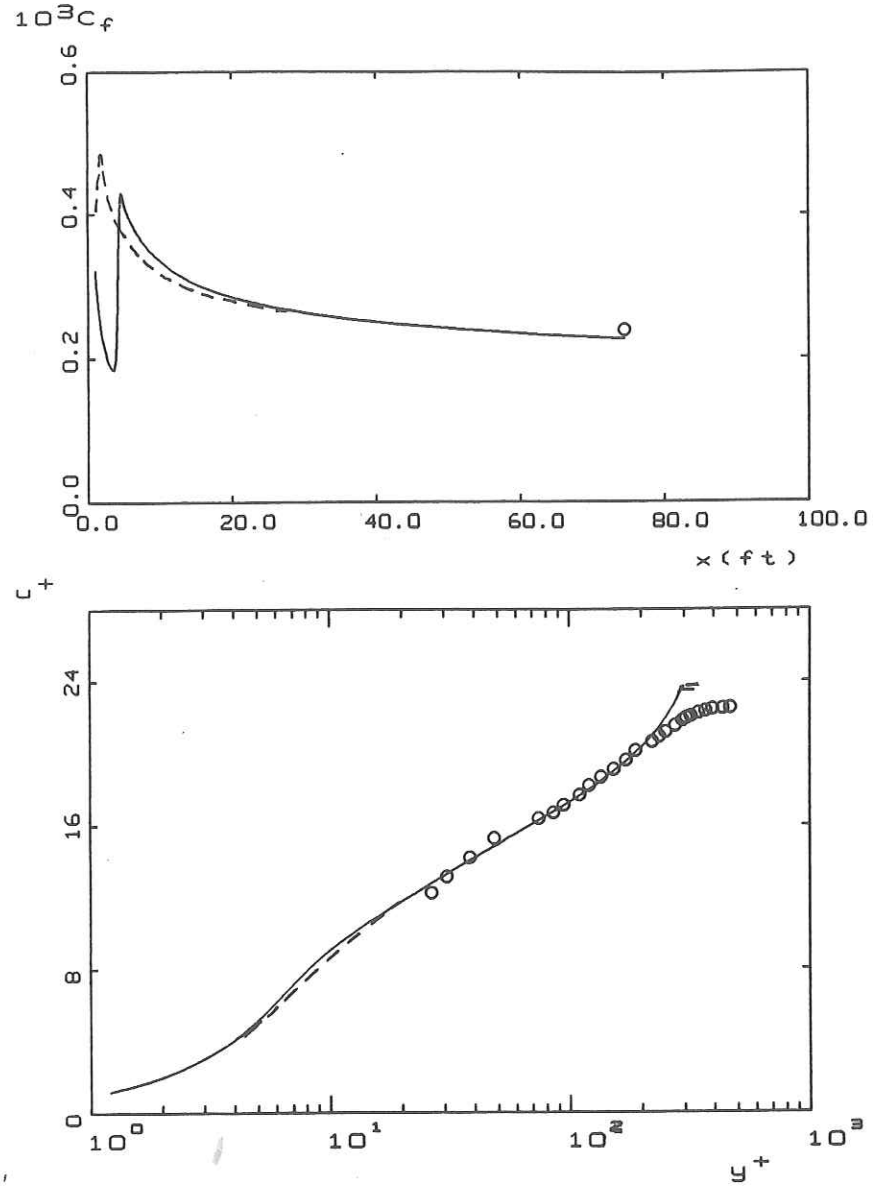

Figure 3.9: Mach 10.31 adiabatic-wall flat-plate boundary layer; o Watson; -- $k-\omega$ with viscous corrections; — — — $k-\omega$ without viscous corrections.

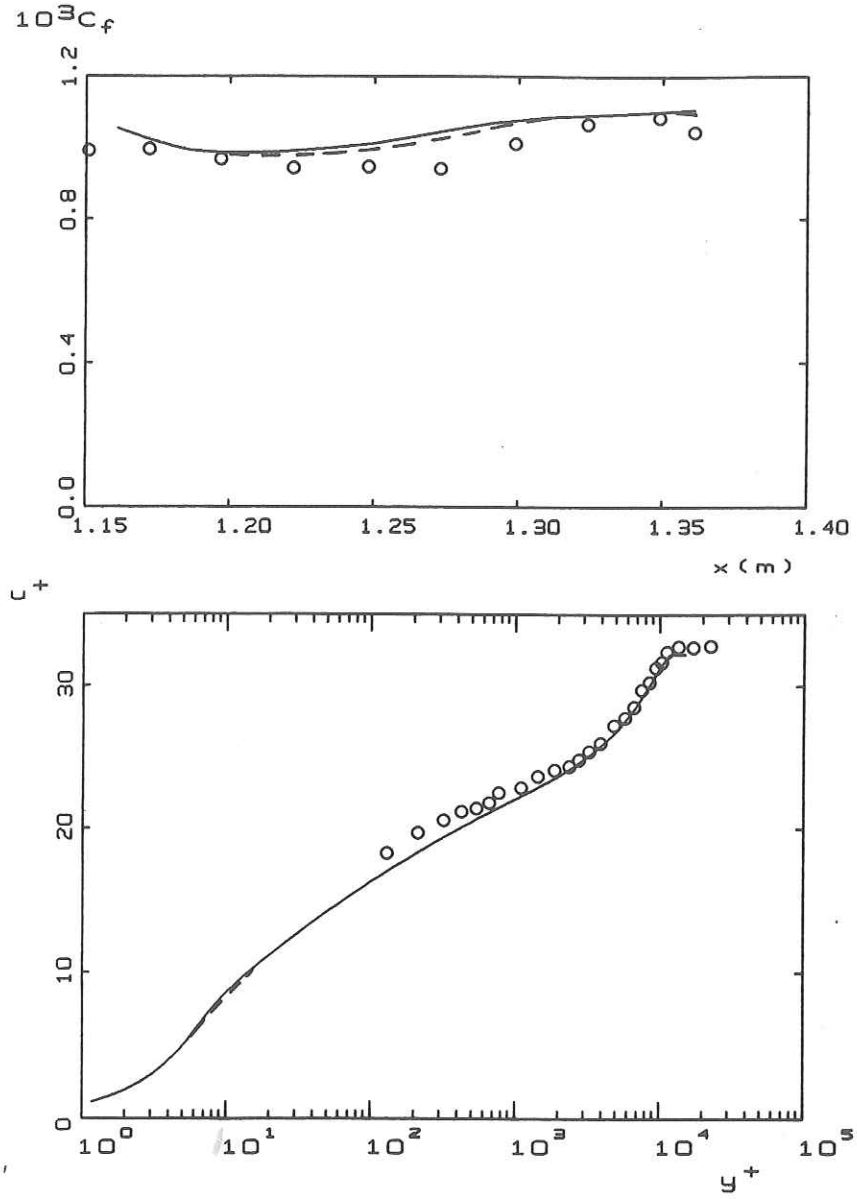

Figure 3.10: Mach 2.563 adiabatic-wall boundary layer; o Fernando-Smits; — $k-\omega$ with viscous corrections; – – – $k-\omega$ without viscous corrections.

Chapter 4

Transitional Boundary-Layer Applications

In order to test the suitability of the low-Reynolds-number $k-\omega$ model for transitional boundary-layers, we have computed all of the two-dimensional transitional boundary layer cases considered by Singer, et al.[9] Table 4.1 summarizes the cases we have done.

Table 4.1: Transitional Boundary Layer Test Cases

Flow	Description	∇p	Data Source
1	Incompressible Flat Plate	None	Schubauer-Klebanoff[22]
2	Favorable ∇p	Favorable	Blair-Werle[23]
3	Supersonic Cone Flow	None	Fisher-Dougherty[25]
3	Supersonic Cone Flow	None	Chen, et al[24]
4	Freestream Turbulence	None	Schubauer-Skramstad[26]
4	Freestream Turbulence	None	Blair[27]
5	Prolate Spheroid	Favorable	Meier-Kreplin-Ming[29]
6	Concave Surface	None	Swearingen-Blackwelder[28]

As discussed by Wilcox[10], transition predictions with the $k-\omega$ model are sensitive to the freestream values of k and ω, most notably to the former. All of the computations have been done using the following boundary condition at

the start of the computation:

$$\frac{\omega_e^{-1}}{\delta}\sqrt{\frac{k_e}{0.3}} = 0.01 \tag{4.1}$$

where δ denotes boundary layer thickness, and subscript e denotes boundary-layer edge. Because our goal is to examine model predictions in the transition region as opposed to predicting the actual transition point, the freestream turbulence level has been selected to match the measured transition location for most of the computations. We quote the initial value of the freestream intensity, T', for all cases, where

$$T' = 100\sqrt{\frac{2}{3}\frac{k_e}{U_e^2}} \tag{4.2}$$

The quantity U_e is boundary-layer edge velocity. The freestream values of k and ω vary throughout the computation, and follow from solution of the model equations in the freestream. See Wilcox[1] for additional details.

In all cases, computation begins at the plate leading edge, and the turbulence kinetic energy is initially set to the freestream value throughout the boundary layer. The initial ω profile is given by the exact laminar-flow solution to the model equations.[10]

Incompressible Flat Plate. The first case is Flow 1 from Singer, et al.[9] This is an incompressible flat-plate boundary layer that undergoes transition at a plate length between 1.6 m. and 1.8 m. The initial freestream intensity is assumed to be 0.043%, and decreases with distance along the plate since the solution to the model equations in the freestream tells us the turbulence decays. At the end of the computation the freestream intensity has dropped to 0.025%. The nominal value quoted for the experiment is 0.030%.

Figure 4.1 compares computed and measured skin friction throughout the transition region. Computed and measured c_f differ by less than 14% of the peak skin friction. According to Singer, et al, the Dey-Narasimha[29] correlation yields values about 6% lower than measured for this flow while the ONERA/CERT[30] model predicts peak skin friction about 25% higher than measured.

Favorable Pressure Gradient Boundary Layers. The next applications are for incompressible boundary layers in a favorable pressure gradient. The boundary layers considered correspond to Flow 2/Cases 1 and 2 of Singer, et al. In addition to having adverse pressure gradient, the surface is cooled. Figure 4.2 compares computed and measured Stanton number for the two cases. Case 2 has a stronger favorable pressure gradient than Case 1. The initial freestream turbulence intensities required to match the measured transition point are 0.61% and 0.91%, respectively, for Cases 1 and 2.

Singer, et al show that the Dey-Narasimha and the ONERA/CERT models are almost as close to the data as the $k-\omega$ prediction, although both predict a more rapid approach to the turbulent state. By contrast, for Case 2 the Dey-

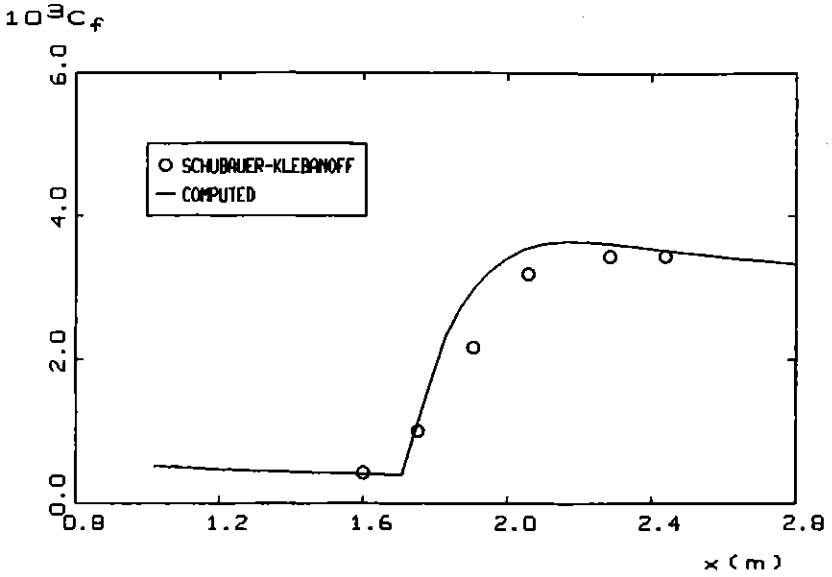

Figure 4.1: Transitional incompressible flat-plate boundary layer.

Narasimha model predicts a peak Stanton number nearly double the measured value. Also, the ONERA/CERT model fails to predict transition for Case 2.

Both of these flows have a very high measured freestream turbulence level (2.0%), which probably accounts for the departure of the skin friction from the laminar value ahead of transition. This is probably buffeting and it tends to smear the Stanton number distribution. While the $k-\omega$ model prediction fails to duplicate this feature, the computation predicts an asymptote to the fully turbulent value in a sensible distance. By contrast, the Dey-Narasimha model does not approach the data until about 1.5 m.

Supersonic Cone Flow. For this application we consider Flow 3 of the Singer, et al study. Cases 1-4 focus on flow past a 5° half angle cone with Mach numbers ranging from 1.16 to 1.86, corresponding to measurements of Fisher and Dougherty.[25] Measurements are available only for the beginning and end of transition. Table 4.2 summarizes the freestream turbulence intensity used, transition Reynolds number, Re_{x_t}, and Reynolds number based on transition width, $Re_{\Delta x_t}$.

Cases 5-7 are for Mach 3.36 flow past a 5° half-angle cone, with an adiabatic surface. The three cases considered have different unit Reynolds numbers. Figure 4.3 compares computed and measured recovery factor, r, for the three cases; freestream turbulence intensity in the computations is 0.1% for all three cases. Note that unit Reynolds number is smallest for Case 5 and largest for Case 7. Interestingly, consistent with measurements, the asymptotic value of

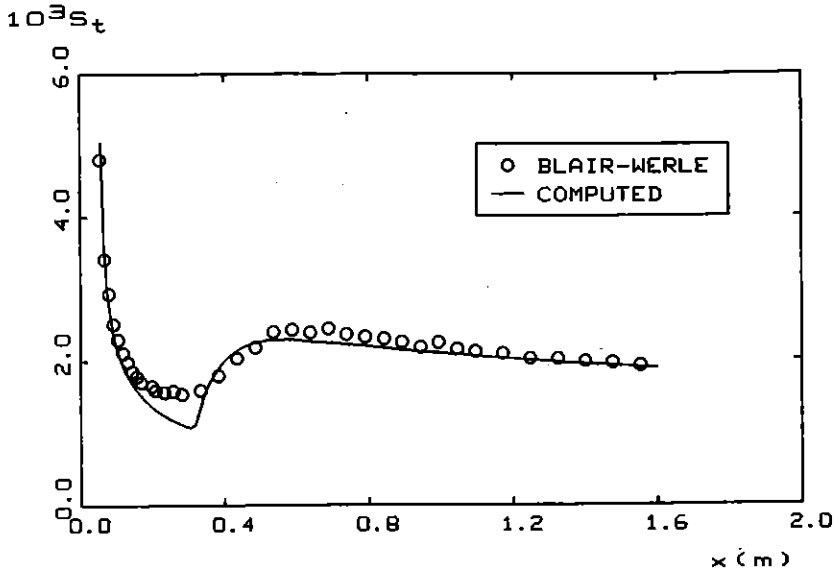

Case 1: Mildly favorable pressure gradient

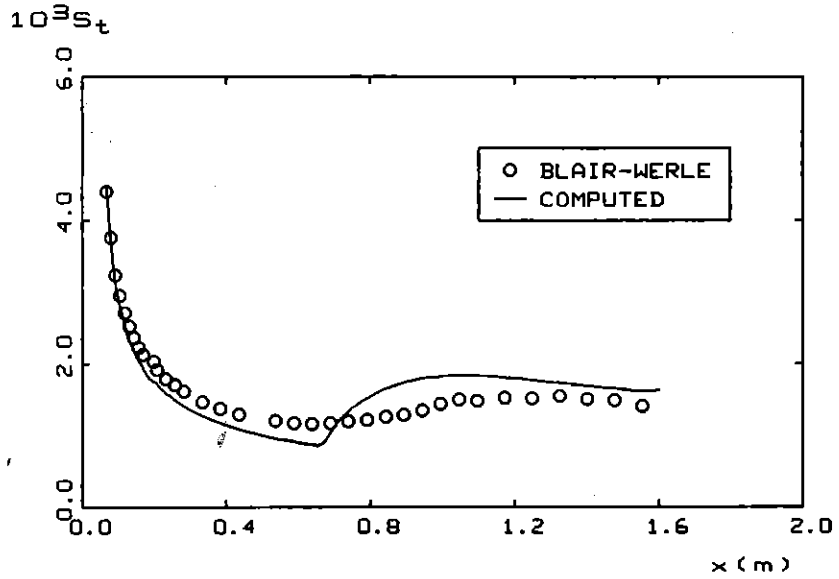

Case 2: Strongly favorable pressure gradient

Figure 4.2: Transitional incompressible boundary-layer flow with favorable pressure gradient and surface cooling.

Table 4.2: Results for Fisher-Dougherty Test Cases

Case	Mach Number	T'	Rex_t	$Re_{\Delta x_t}$	$(Re_{\Delta x_t})_{exp}$
1	1.16	.0020%	$7.02 \cdot 10^6$	$0.89 \cdot 10^6$	$0.69 \cdot 10^6$
2	1.30	.0075%	$5.61 \cdot 10^6$	$0.84 \cdot 10^6$	$0.97 \cdot 10^6$
3	1.55	.0027%	$7.89 \cdot 10^6$	$1.08 \cdot 10^6$	$1.24 \cdot 10^6$
4	1.86	.0073%	$7.29 \cdot 10^6$	$1.07 \cdot 10^6$	$1.56 \cdot 10^6$

the recovery factor is about 0.875 for all three cases compared to the generally accepted value of 0.89. By contrast, the Dey-Narasimha and ONERA/CERT models predict an asymptotic value in excess of 0.88. As a simple numerical experiment, we have run these computations without transverse curvature, i.e., as two-dimensional flows. The asymptotic value of the recovery factor is 0.89.

Freestream Turbulence Effects. We turn now to effects of freestream turbulence, i.e., Flow 4 of the Singer, et al study. All of the cases considered are for incompressible boundary layers. Table 4.3 shows that computed transition width for Cases 1-5 is consistently smaller than measured, especially at the smallest transition Reynolds numbers. Note that the measured freestream turbulence intensity has been used in the computations.

Table 4.3: Results for Schubauer-Skramstad Test Cases

Case	T'	Rex_t	$Re_{\Delta x_t}$	$(Re_{\Delta x_t})_{exp}$
1	.042%	$2.85 \cdot 10^6$	$0.88 \cdot 10^6$	$1.00 \cdot 10^6$
2	.100%	$2.75 \cdot 10^6$	$0.86 \cdot 10^6$	$1.20 \cdot 10^6$
3	.200%	$2.20 \cdot 10^6$	$0.78 \cdot 10^6$	$1.50 \cdot 10^6$
4	.260%	$1.80 \cdot 10^6$	$0.69 \cdot 10^6$	$1.40 \cdot 10^6$
5	.340%	$1.40 \cdot 10^6$	$0.58 \cdot 10^6$	$1.25 \cdot 10^6$

For Cases 6, 7 and 8, Figure 4.4 shows that predicted peak skin friction is about 10%-15% lower than measured. The ONERA/CERT model's peak skin friction is about 5%-10% higher than measured, while the Dey-Narasimha model yields peak skin friction that is 20%-25% higher than measured. As with Cases 1-5, the computations match the measured freestream turbulence intensity, which is 0.25%, 1.00% and 2.00% for Cases 6, 7 and 8, respectively.

Incompressible Flow Past a Spheroid. This case is Flow 5 from Singer, et al. The flow examines the effect of a roughness strip on the transition of a boundary layer over a prolate spheroid at zero angle of attack. Experimental data have been provided by Meier, Kreplin and Ming.[29] Table 4.4 summarizes the four cases, including the value of T' used in the computations.

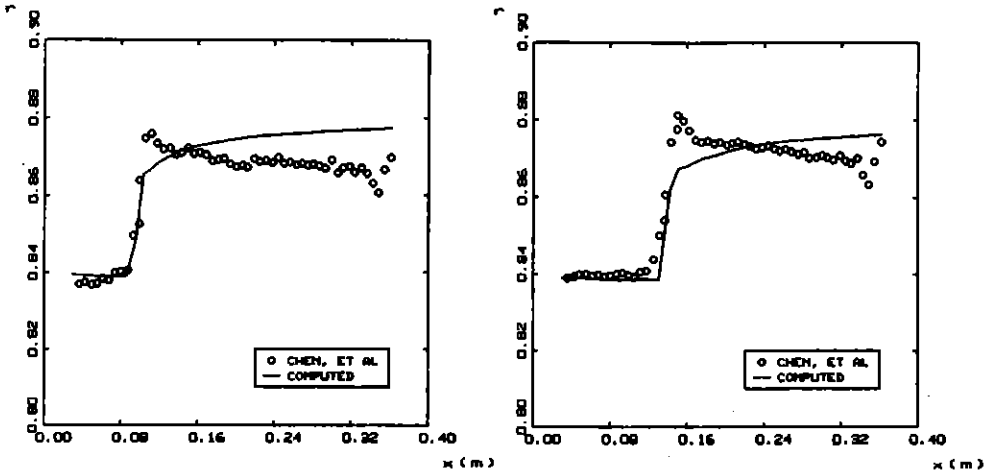

Case 5 Case 6

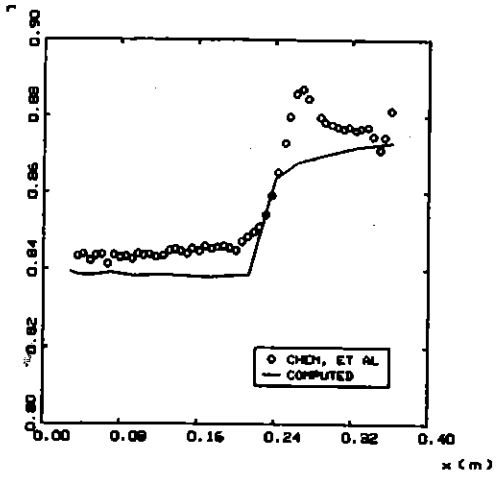

Case 7

Figure 4.3: Transitional flow on a 5° half-angle, adiabatic cone at Mach 3.36.

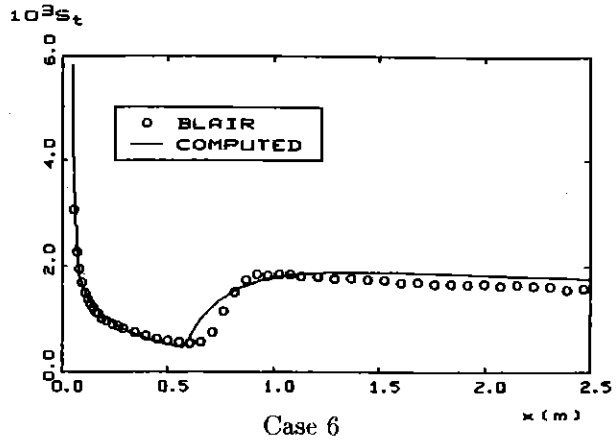

Case 6

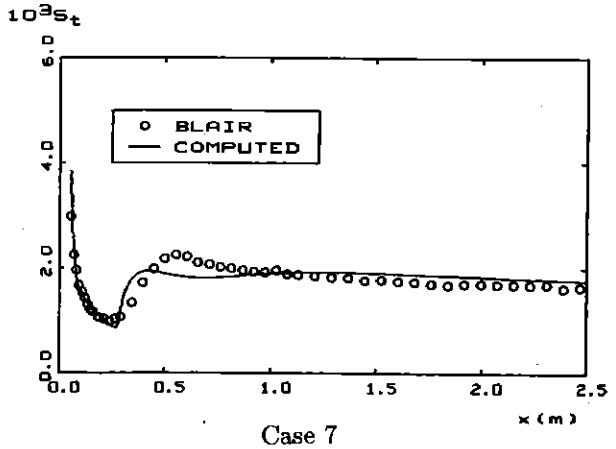

Case 7

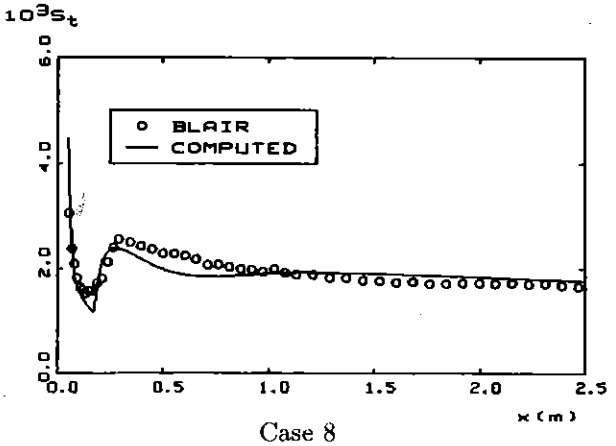

Case 8

Figure 4.4: Transition width for flat-plate boundary layers.

Figures 4.5 through 4.8 compare computed and measured skin friction (based on local boundary-layer edge velocity) as a function of arc length along the spheroid. As shown, computed and measured skin friction are closest when transition is induced by the roughness strip. Without the roughness strip, the predicted transition occurs more abruptly than measured.

Table 4.4: Meier-Kreplin-Ming Test Cases

Case	Description	T'
1	$U_\infty = 20$ m/sec, no roughness strip	.017%
2	$U_\infty = 20$ m/sec, with roughness strip	.153%
3	$U_\infty = 30$ m/sec, no roughness strip	.010%
4	$U_\infty = 30$ m/sec, with roughness strip	.115%

Concave Surface Boundary Layer The final application is for incompressible flow over a concave surface. Because the physical flow has longitudinal vortices, this application would be more appropriately done in a three-dimensional computation. Nevertheless, following Singer, et al, we present results of a two-dimensional computation in Figure 4.9. Freestream turbulence intensity in the computation is 1.21%. The strongest statement we can make is that the peak value of c_f matches the measured value. The Dey-Narasimha and ONERA/CERT models yield peak values about 6% and 16% higher than measured, respectively.

In summary, while the differences between computed and measured skin friction and Stanton number are less than those with the Dey-Narasimha and ONERA/CERT models, the formulation is imperfect. This is most evident for the cases with large transition Reynolds numbers. In these cases, the model-predicted transition occurs more abruptly than measured, especially for the compressible cases. Chapter 5 explains why this is true and shows that a better choice of the low-Reynolds-number closure coefficients R_k and R_ω may reconcile the differences.

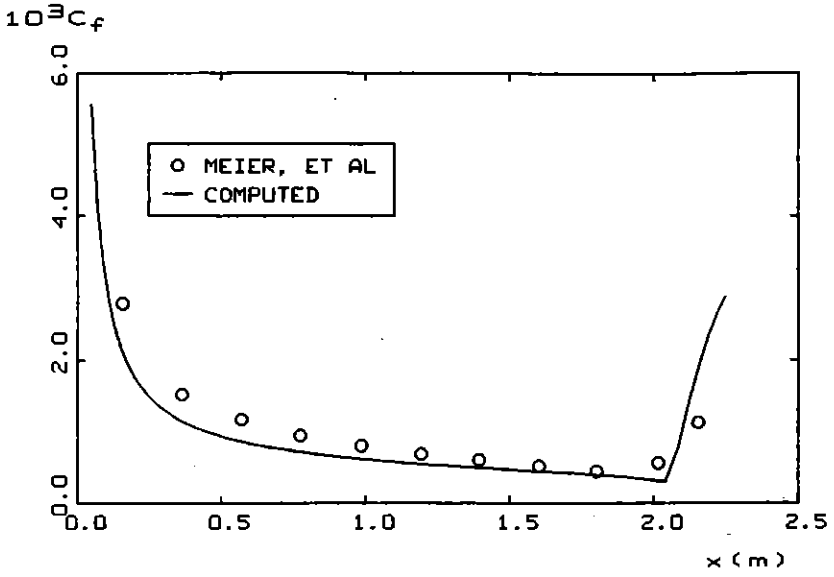

Figure 4.5: Flow past a prolate spheroid; $U_\infty = 20$ m/sec; no roughness strip.

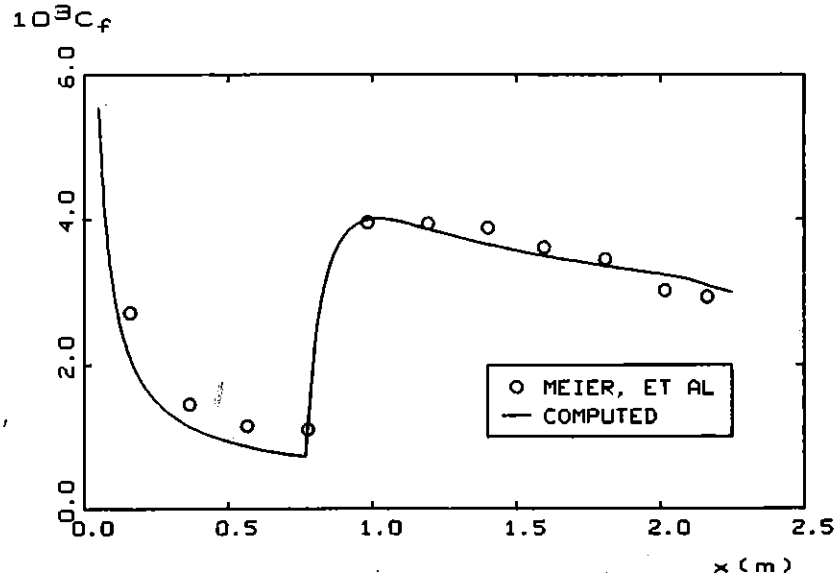

Figure 4.6: Flow past a prolate spheroid; $U_\infty = 20$ m/sec; with roughness strip.

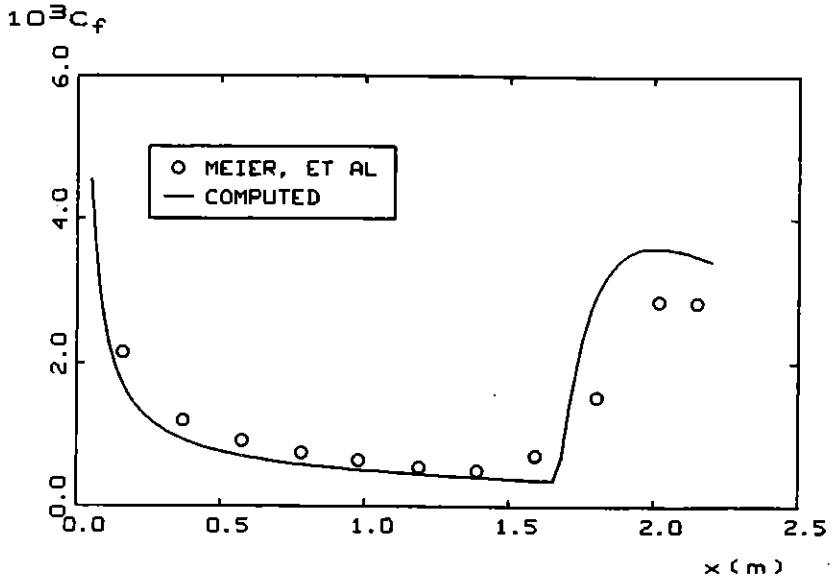

Figure 4.7: Flow past a prolate spheroid; $U_\infty = 30$ m/sec; no roughness strip.

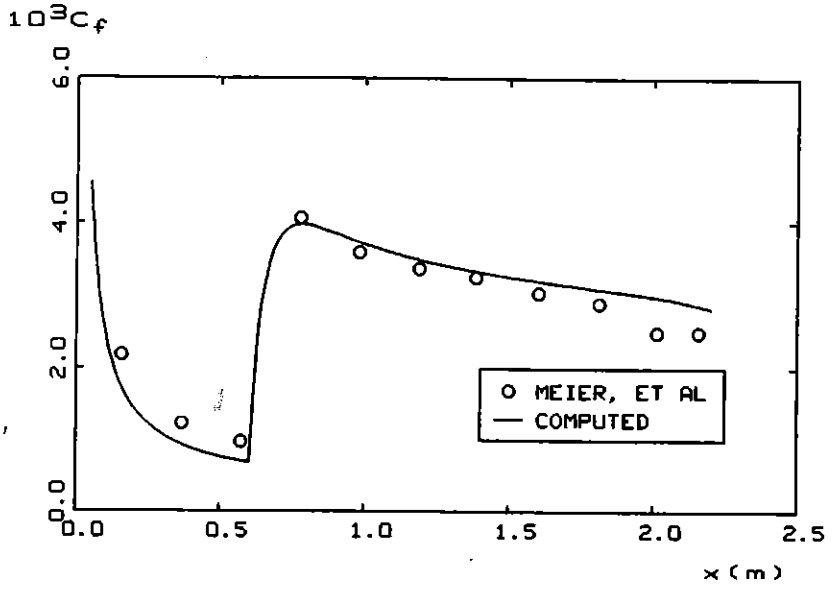

Figure 4.8: Flow past a prolate spheroid; $U_\infty = 30$ m/sec; with roughness strip.

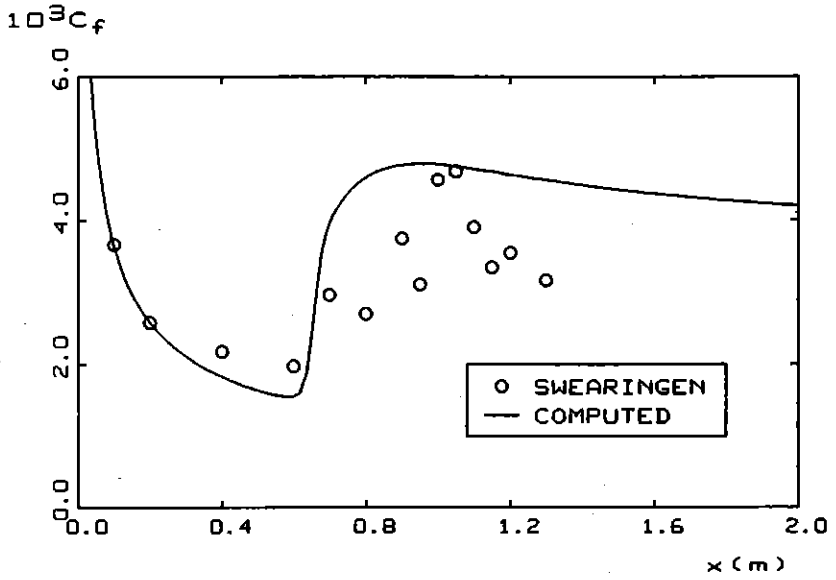

Figure 4.9: Transitional flow on a concave surface; incompressible flow.

Chapter 5

Boundary Condition and Closure Coefficient Sensitivity

In this chapter, we investigate the sensitivity of $k-\omega$ model solutions to the freestream value of ω. The sensitivity is related to the physical time scales relevant in shear flows. A solution similar to Menter's postulate has been tested. Additionally, we have determined the sensitivity of model-predicted transition width to the low-Reynolds-number closure coefficients. We have found that transition width is insensitive to three of the postulated low-Reynolds-number closure coefficients (α_o, α_o^* and R_β) and is strongly affected by two others (R_k and R_ω). As a result of the understanding gained, we have found an ad hoc modification that yields more realistic transition width for high transition Reynolds numbers.

5.1 Boundary Condition Sensitivity

Unlike other two-equation models, the $k-\omega$ model reflects a sensitivity to freestream turbulence. This sensitivity is physically realistic for boundary layers as turbulent boundary-layer skin friction is known to increase with increasing freestream turbulence level. The model does indeed predict an increase in skin friction. However, the model also predicts a strong effect of the freestream value of ω on the spreading rate of mixing layers, jets and wakes. Measurements do not suggest such sensitivity. Finally, the sensitivity mitigates one of the $k-\omega$ model's strongest assets in transition prediction, viz, the ease with which initial profiles can be established. While the ω equation has a well-defined laminar flow solution, the solution is somewhat sensitive to the freestream value of ω.

Hence, transition predictions are affected by the model's sensitivity to freestream boundary conditions.

Recall that for fully turbulent flows, the high-Reynolds-number $k-\omega$ model postulates that the Reynolds shear stress is given by

$$-\overline{u'v'} = \frac{k}{\omega}\frac{\partial u}{\partial y} \tag{5.1}$$

As we approach the freestream, we expect on physical grounds that k and $\overline{u'v'}$ approach negligibly small values for a fully turbulent boundary layer. It is possible to achieve this according to Equation (5.1) even with a small freestream value of ω, provided the ratio of k to ω remains small.

Having the ratio of k to ω small is not the only physical consideration regarding a possible lower bound on the freestream value of ω. To understand why, note that the quantity ω is the reciprocal of the time it takes the turbulence to adjust to changes in its environment. By contrast, the mean velocity gradient, $\partial u/\partial y$, is the reciprocal of the time scale on which the mean flow is changing. The Reynolds averaging procedure used to arrive at our model equations implicitly assumes that mean-flow properties are not changing more rapidly than the turbulent fluctuations. Hence, we have made an implicit assumption that in a shear flow,

$$\omega_{min} > \left|\frac{\partial u}{\partial y}\right| \tag{5.2}$$

Menter[31] has shown that by computing the Reynolds shear stress according to

$$-\overline{u'v'} = \min\left[\frac{k}{\omega}\ ,\ \frac{0.3k}{\partial u/\partial y}\right]\frac{\partial u}{\partial y} \tag{5.3}$$

$k-\omega$ model predictions can be brought into closer agreement with measurements for some flows. This is tantamount to saying that

$$\omega_{min} = \frac{10}{3}\left|\frac{\partial u}{\partial y}\right| \tag{5.4}$$

when computing the eddy viscosity.

Of course, Menter's correction was designed to improve the model's predictions for separated flows, rather than to address boundary condition sensitivity. Nevertheless, we have considered the possibility that Menter's correction may also remove some of the sensitivity. To do so, we have tested Menter's proposal for flat-plate boundary layer flow and the turbulent far wake. We have found that the Menter correction does very little to remove the model's sensitivity to the freestream value of ω for either flow.

While it is easy to implement, this approach is not entirely self consistent. We are still permitting ω to assume values less than ω_{min} and simply adjusting

the eddy viscosity according to Equation (5.3). To eliminate the inconsistency, we can define a modified specific dissipation rate, $\bar{\omega}$, according to:

$$\bar{\omega} = \max\left[\omega, \lambda\frac{\partial u}{\partial y}\right] \tag{5.5}$$

where λ is a coefficient to be determined. The eddy viscosity, k equation and ω equation then become

$$\mu_T = \alpha^*\frac{\rho k}{\bar{\omega}} \tag{5.6}$$

$$\frac{\partial}{\partial t}(\rho k) + \frac{\partial}{\partial x_j}(\rho u_j k) = \tau_{ij}^T\frac{\partial u_i}{\partial x_j} - \beta^*\rho\bar{\omega}k + \frac{\partial}{\partial x_j}\left[(\mu + \sigma^*\mu_T)\frac{\partial k}{\partial x_j}\right] \tag{5.7}$$

$$\frac{\partial}{\partial t}(\rho\omega) + \frac{\partial}{\partial x_j}(\rho u_j\omega) = \alpha\frac{\omega}{k}\tau_{ij}^T\frac{\partial u_i}{\partial x_j} - \beta\rho\bar{\omega}\omega + \frac{\partial}{\partial x_j}\left[(\mu + \sigma\mu_T)\frac{\partial\omega}{\partial x_j}\right] \tag{5.8}$$

Using $\lambda \leq 2$, this modification has virtually no effect on solutions. However, when $\lambda \geq 3$, boundary-layer solutions exhibit no sensitivity to the freestream value of ω. However, this prescription is completely ineffective for the far wake. Consequently, we are still seeking a satisfactory resolution of the model's freestream boundary condition sensitivity.

5.2 Closure Coefficient Sensitivity

Turning now to closure-coefficient sensitivity, we have found that when transition occurs at relatively low Reynolds numbers (i.e., typically for $Re_{x_t} < 10^6$) the predicted extent of the transition region is consistent with measurements. By contrast, at higher transition Reynolds numbers, predicted transition width generally is smaller than measured. This problem is especially noticeable for compressible boundary layers. For example, Figure 5.1 compares computed and measured Stanton number, St, for Mach 20 flow[32] past a 5° half-angle cone. As shown, the computed Stanton number increases much more abruptly than measured.

To understand why the low-Reynolds-number version of the $k-\omega$ model underpredicts transition width at high Reynolds number, recall that the boundary-layer form of the equations for k and ω are:

$$\rho u\frac{\partial k}{\partial x} + \rho v\frac{\partial k}{\partial y} = \mu_T\left(\frac{\partial u}{\partial y}\right)^2 - \beta^*\rho\omega k + \frac{\partial}{\partial y}\left[(\mu + \sigma^*\mu_T)\frac{\partial k}{\partial y}\right] \tag{5.9}$$

$$\rho u\frac{\partial\omega}{\partial x} + \rho v\frac{\partial\omega}{\partial y} = \alpha\frac{\omega}{k}\mu_T\left(\frac{\partial u}{\partial y}\right)^2 - \beta\rho\omega^2 + \frac{\partial}{\partial y}\left[(\mu + \sigma\mu_T)\frac{\partial\omega}{\partial y}\right] \tag{5.10}$$

$$\mu_T = \alpha^*\frac{\rho k}{\omega} \tag{5.11}$$

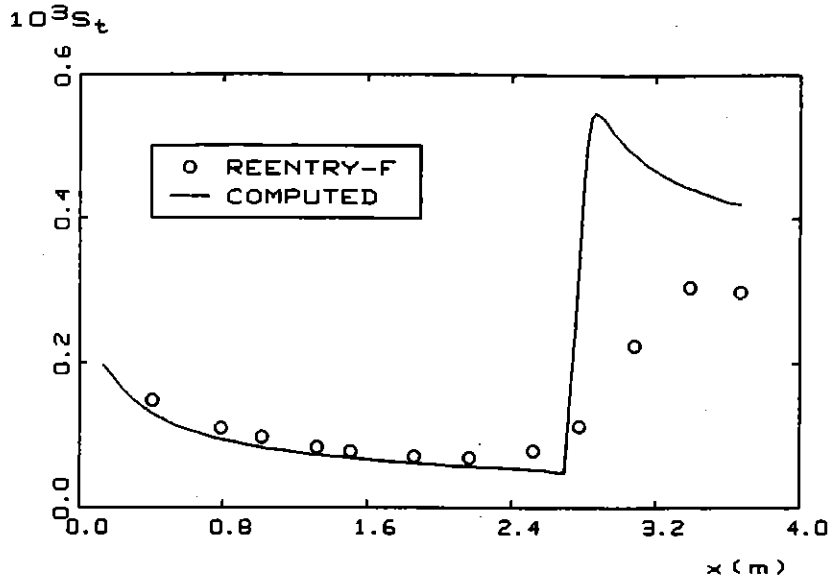

Figure 5.1: Mach 20 flow past a 5° half-angle cone.

Additionally, the closure coefficients α^*, α, β^*, β, σ^* and σ are given by Equations (2.12-2.17). Inspection of Equations (5.9)-(5.11) shows that the five low Reynolds number specific closure coefficients, α_o, α_o^*, R_β, R_k and R_ω accomplish two ends. First, α_o^* and α_o control the points at which k and ω are amplified. The coefficients R_β, R_k and R_ω control the rate at which α, α^* and β^* approach their fully turbulent values.

Closer examination of solutions to Equations (5.9)-(5.11) reveals that the primary role of R_β is to establish the peak value of k in the fully turbulent region. However, it plays a more or less passive role in the transition region. Decreasing the value of R_β tends to increase the predicted width of the transition zone slightly.

The value of α_o^* has been chosen to guarantee that small disturbances begin to be amplified at the minimum critical Reynolds number for the Blasius boundary layer. At low Reynolds numbers, the value of α_o determines the width of the transition zone. To understand this, recall from Wilcox[10] that for the Blasius boundary layer, the production terms in the k and ω equations first exceed their corresponding dissipation terms at the following "critical" Reynolds numbers.

$$(Re_x)_k = \frac{8100}{\alpha_o^*} \tag{5.12}$$

$$(Re_x)_\omega = \frac{12150}{\alpha_o} \tag{5.13}$$

If we approximate that the dominant mechanism in the early stages of transition is the balance amongst the streamwise convection, production and dissipation terms, the k and ω equations simplify to

$$u\frac{dk}{dx} = \frac{\beta}{3}\left[\frac{3\alpha_o^*}{\beta}\left(\frac{\partial u/\partial y}{\omega}\right)^2 - 1\right]k\omega \tag{5.14}$$

$$u\frac{d\omega}{dx} = \beta\left[\frac{5}{9}\frac{\alpha_o}{\beta}\left(\frac{\partial u/\partial y}{\omega}\right)^2 - 1\right]\omega^2 \tag{5.15}$$

Since the ratio of $\partial u/\partial y$ to ω increases as $Re_x^{1/2}$ for the Blasius boundary layer, the following observations can be made. **First**, provided α_o^* and α_o are chosen such that k is amplified before ω is amplified, k will grow with increasing values of x beyond $(Re_x)_k$. **Second**, the value of α_o controls the location at which ω begins to grow, which ultimately terminates the growth of k, i.e., determines the end of transition. **Third**, when the transition Reynolds number is of the order of $1 \cdot 10^6$, the difference between $(Re_x)_k$ and $(Re_x)_\omega$ is roughly 7% of the measured width of the transition region. **Fourth**, as the transition Reynolds number increases, the difference between $(Re_x)_k$ and $(Re_x)_\omega$ becomes a much smaller fraction of the transition width.

Hence, we should expect the relative values of α_o^* and α_o to have little effect on the width of the transition zone at high Reynolds numbers. Numerical experimentation confirms that at high Reynolds numbers, transition width is essentially independent of the values of α_o^* and α_o.

We have also examined the sensitivity of transition width to the two remaining low Reynolds number closure coefficients, R_k and R_ω. In contrast to the relative insensitivity to values of the other three low Reynolds number parameters, transition width is very strongly affected by R_k and R_ω. Figure 5.2 illustrates the effect of tripling the values of R_k and R_ω for the Mach 20 flow discussed above. Interestingly, not only is the transition width more accurately represented, so is the heat transfer in the fully turbulent region.

This exercise, although ad hoc in nature, points to a possible resolution of the model's inaccuracy for transition width at high Reynolds numbers. There are indeed pairs of values of R_k and R_ω, other than those quoted in Equation (2.16), that yield satisfactory results for general boundary-layer applications. Alternative values follow from a perturbation analysis of the viscous sublayer. Such analysis is the topic of the next chapter.

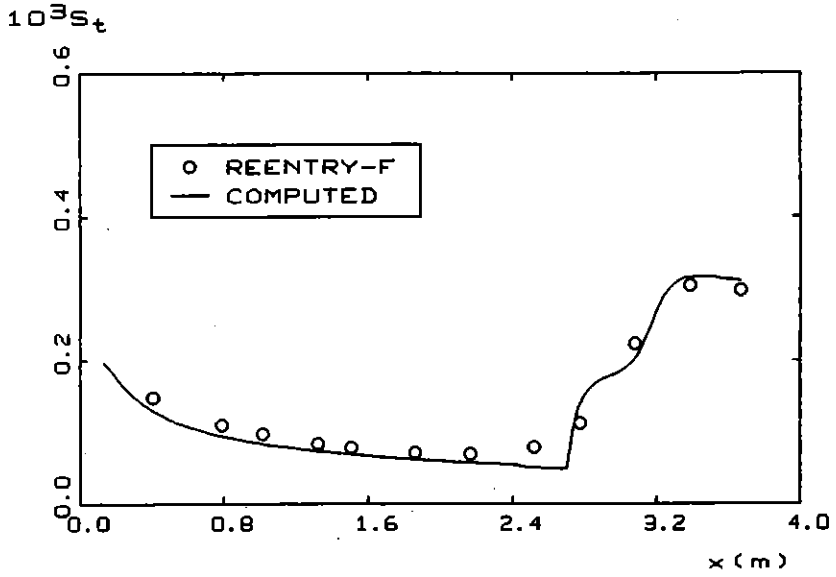

Figure 5.2: Mach 20 flow past a 5° half-angle cone with $R_k = 18$ and $R_\omega = 8.1$.

Chapter 6

Singular Perturbation Analysis of the Compressible Turbulent Boundary Layer

As shown in Chapter 4, the low-Reynolds-number $k-\omega$ model yields transition predictions consistent with incompressible flat-plate boundary layer measurements, including sensitivity to freestream turbulence intensity. While the model provides a realistic simulation of the transitional region at high freestream turbulence levels (e.g., $> 0.5\%$ freestream intensity), the model predicts more abrupt than measured transition for smaller turbulence levels. As shown in Chapter 5, the model displays a strong (possibly nonphysical) sensitivity to freestream turbulence properties for free shear flows. The sensitivity is present for boundary layers as well, although the effect is not as pronounced (no more than 10% changes in skin friction, for example) as it is for free shear flows.

For all three cases, viz, transitional boundary layers, free shear flows and turbulent boundary layers, sensitivity to freestream turbulence is felt through the entrainment process at the turbulent/nonturbulent interface. Specific to the transitional case, we usually speak of the boundary layer's *receptivity*. Clearly, developing a satisfactory engineering model for describing the transition process requires a satisfactory description of the boundary layer's receptivity to freestream disturbances.

In order to analyze this phenomenon, the ideal tool is a perturbation solution for the turbulent boundary layer. Wilcox[1] has done such a solution for incompressible flow, including effects of pressure gradient. Since our goal in this Contract is to develop a model for compressible flows, a compressible defect-layer

solution is needed. Hence, we have initiated development of such a solution.

As shown by Wilcox,[33] the perturbation analysis develops an inner expansion corresponding to the viscous sublayer and an outer expansion corresponding to the defect layer. In this chapter, we examine the viscous sublayer solution first.

6.1 The Viscous Sublayer

Our primary motivation for analyzing the compressible sublayer is to help quantify solution sensitivity to R_k and R_ω when compressibility effects are significant. The most important issue is to determine the effect of compressibility on the model predicted form of the compressible law of the wall, i.e., the Kármán constant, κ, and the additive constant, B.

In addition to affecting the width of the transition region, the closure coefficients R_k and R_ω determine the value of the constant in the law of the wall, B, for a turbulent boundary layer. In fact, there exist unique pairs of values (R_k, R_ω) that yield $B = 5.0$ for the incompressible sublayer. The appropriate values have been established by using perturbation methods to solve the sublayer equations and to determine B from the limiting form of the solution as $y^+ \to \infty$.

Results of the Mach 20 transition application above suggest that larger values of R_k and R_ω may be more appropriate. However, there is a possibility that larger values may be appropriate only for high Mach number flows. To determine effects of compressibility, we have redone our perturbation analysis of the viscous sublayer with effects of compressibility included.

For compressible flow, the sublayer equations assume the following form.

$$\frac{d}{dy}\left[(\mu+\mu_T)\frac{du}{dy}\right] = 0 \tag{6.1}$$

$$\frac{d}{dy}\left[(\mu+\mu_T)\,u\frac{du}{dy} + \left(\frac{\mu}{Pr_L}+\frac{\mu_T}{Pr_T}\right)\frac{dh}{dy} + (\mu+\sigma^*\mu_T)\frac{dk}{dy}\right] = 0 \tag{6.2}$$

$$\frac{d}{dy}\left[(\mu+\sigma^*\mu_T)\frac{dk}{dy}\right] + \mu_T\left(\frac{du}{dy}\right)^2 - \beta^*\rho\omega k = 0 \tag{6.3}$$

$$\frac{d}{dy}\left[(\mu+\sigma\mu_T)\frac{d\omega}{dy}\right] + \alpha\alpha^*\rho\left(\frac{du}{dy}\right)^2 - \beta\rho\omega^2 = 0 \tag{6.4}$$

where

$$\mu_T = \alpha^*\rho k/\omega \quad \text{and} \quad \rho h = \rho_w h_w \tag{6.5}$$

We can integrate Equations (6.1 and (6.2) once, wherefore

$$(\mu+\mu_T)\frac{du}{dy} = \rho_w u_\tau^2 \tag{6.6}$$

$$(\mu+\mu_T)\,u\frac{du}{dy}+\left(\frac{\mu}{Pr_L}+\frac{\mu_T}{Pr_T}\right)\frac{dh}{dy}+(\mu+\sigma^*\mu_T)\,\frac{dk}{dy}=-q_w \tag{6.7}$$

where u_τ is friction velocity, ρ_w is density at the surface, and q_w is surface heat flux. We make these equations dimensionless by introducing the following variables.

$$u^+=\frac{u}{u_\tau},\quad y^+=\frac{u_\tau y}{\nu_w},\quad k^+=\frac{k}{u_\tau^2} \tag{6.8}$$

$$\rho^+=\frac{\rho}{\rho_w},\quad h^+=\frac{h}{u_\tau^2},\quad \omega^+=\frac{\nu_w\omega}{u_\tau^2} \tag{6.9}$$

$$\mu^+=\frac{\mu}{\mu_w},\quad \mu_T^+=\frac{\mu_T}{\mu_w} \tag{6.10}$$

The resulting equations are:

$$\left(\mu^+ + \mu_T^+\right)\frac{du^+}{dy^+}=1 \tag{6.11}$$

$$\left(\frac{\mu^+}{Pr_L}+\frac{\mu_T^+}{Pr_T}\right)\frac{dh^+}{dy^+}=-q_w^+-u^+-\left(\mu^+ + \sigma^*\mu_T^+\right)\frac{dk^+}{dy^+} \tag{6.12}$$

$$\frac{d}{dy^+}\left[\left(\mu^+ + \sigma^*\mu_T^+\right)\frac{dk^+}{dy^+}\right]+\mu_T^+\left(\frac{du^+}{dy^+}\right)^2-\beta^*\rho^+\omega^+k^+=0 \tag{6.13}$$

$$\frac{d}{dy^+}\left[\left(\mu^+ + \sigma\mu_T^+\right)\frac{d\omega^+}{dy^+}\right]+\alpha\alpha^*\rho^+\left(\frac{du^+}{dy^+}\right)^2-\beta\rho^+(\omega^+)^2=0 \tag{6.14}$$

$$\mu_T^+=\alpha^*\frac{\rho^+k^+}{\omega^+},\quad \rho^+h^+=h_w^+,\quad q_w^+=\frac{q_w}{\rho_w u_\tau^3} \tag{6.15}$$

This is a sixth order system of coupled nonlinear equations, and we thus need six boundary conditions. Four conditions can be applied at the surface and two for $y^+\to\infty$. Specifically, from no slip, the velocity and turbulence kinetic energy vanish at the surface so that

$$u^+(0)=0 \quad \text{and} \quad k^+(0)=0 \tag{6.16}$$

We can specify either surface temperature or surface heat flux, i.e.,

$$h^+(0)=h_w^+ \quad \text{or} \quad \frac{dh^+}{dy^+}(0)=-Pr_Lq_w^+ \tag{6.17}$$

The final surface boundary condition pertains to the surface value of the specific dissipation rate. We can either use the "rough-wall" boundary condition for

which the surface value of ω is finite or the "smooth-wall" condition in which the asymptotic limiting form for ω is imposed. That is we have:

$$\omega^+(0) = \omega_w^+ \quad \text{or} \quad \omega^+(y^+) \to \frac{6}{\beta(y^+)^2} \text{ as } y^+ \to 0 \tag{6.18}$$

Boundary conditions far from the surface follow from matching to the defect-layer solution or, as demonstrated by Wilcox,[33] by matching to the wall layer solution, which can be obtained in closed form. From the compressible wall layer solution,[34] we thus conclude that

$$\omega^+ \to \frac{1}{\sqrt{\beta_\infty^*}} \frac{du^+}{dy^+} \quad \text{as} \quad y^+ \to \infty \tag{6.19}$$

and

$$\rho^+ k^+ \to \frac{1}{\sqrt{\beta_\infty^*}} - \frac{\gamma - 1}{2} \frac{\sigma^* Pr_T}{\beta_\infty^*} M_\tau^2 \quad \text{as} \quad y^+ \to \infty \tag{6.20}$$

where

$$M_\tau = \left[(\gamma - 1) h_w^+\right]^{-1/2} \tag{6.21}$$

Finally, the velocity in the wall layer is given by

$$\frac{u^*}{u_\tau} = \frac{1}{\kappa} \ell n y^+ + B \tag{6.22}$$

where u^* is the scaled velocity that, in terms of the dimensionless variables is given by

$$\frac{u^*}{u_\tau} = \sqrt{\frac{2h_w^+}{Pr_T}} \left\{ \sin^{-1} \left[\frac{u^+ + q_w^+}{\sqrt{\frac{2h_w^+}{Pr_T} + (q_w^+)^2}} \right] - \sin^{-1} \left[\frac{q_w^+}{\sqrt{\frac{2h_w^+}{Pr_T} + (q_w^+)^2}} \right] \right\} \tag{6.23}$$

We have solved Equations (6.11) through (6.15) subject to Equations (6.16) through (6.21) by modifying our incompressible sublayer program. Computations have been done with the primary focus on the effect of surface temperature on B, which is obtained from the solution as follows.

$$B = \lim_{y^+ \to \infty} \left[u^+ - \frac{1}{\kappa} \ell n y^+ \right] \tag{6.24}$$

As shown in Figure 6.1, for an adiabatic wall and with R_β, R_k and R_ω given by Equation (2.16), there is less than a 10% change in B for h_w^+ varying between 500 and 10,000. Although more computations will be needed to consider all possibilities, it appears that compressibility has a relatively small effect on $k-\omega$ model predicted sublayer structure.

Turning to the ad hoc modification discussed in Chapter 5, the constant in the law of the wall, B, corresponding to using $R_k = 18$ and $R_\omega = 8.1$ is in excess

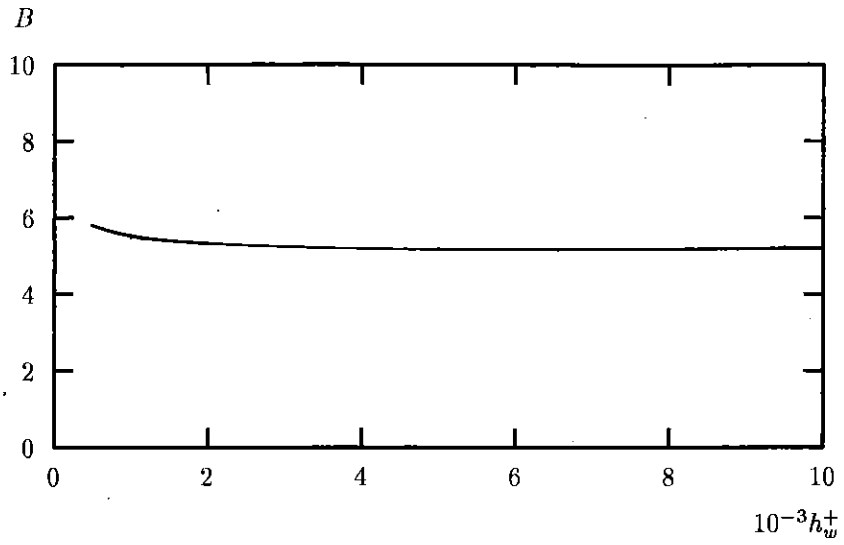

Figure 6.1: Variation of the constant in the law of the wall with surface temperature.

of 10. According to the perturbation solution, the value of B can be reduced to approximately 5.0 by selecting $(R_k, R_\omega) = (18, 28)$ or $(R_k, R_\omega) = (9.5, 8.1)$. Unfortunately, both choices fail to yield a satisfactory solution for the Mach 20 case discussed in Chapter 5. While this cursory examination of the problem does not exhaust all possible choices for R_k and R_ω, it appears that some modification of the damping functions for α^* and α may be needed.

6.2 The Defect Layer

For compressible boundary layers, the $k-\omega$ model equations are as follows.

$$\frac{\partial}{\partial x}(\rho u) + \frac{\partial}{\partial y}(\rho v) = 0 \tag{6.25}$$

$$\rho u\frac{\partial u}{\partial x} + \rho v\frac{\partial u}{\partial y} = -\frac{dp}{dx} + \frac{\partial}{\partial y}\left[(\mu + \mu_T)\frac{\partial u}{\partial y}\right] \tag{6.26}$$

$$\rho u\frac{\partial h}{\partial x} + \rho v\frac{\partial h}{\partial y} = u\frac{dp}{dx} + \mu\left(\frac{\partial u}{\partial y}\right)^2 + \beta^*\rho\omega k + \frac{\partial}{\partial y}\left[\left(\frac{\mu}{Pr_L} + \frac{\mu_T}{Pr_T}\right)\frac{\partial h}{\partial y}\right] \tag{6.27}$$

$$\rho u\frac{\partial k}{\partial x} + \rho v\frac{\partial k}{\partial y} = \mu_T\left(\frac{\partial u}{\partial y}\right)^2 - \beta^*\rho\omega k + \frac{\partial}{\partial y}\left[(\mu + \sigma^*\mu_T)\frac{\partial k}{\partial y}\right] \tag{6.28}$$

$$\rho u\frac{\partial \omega}{\partial x}+\rho v\frac{\partial \omega}{\partial y}=\alpha\rho\frac{\omega}{k}\mu_T\left(\frac{\partial u}{\partial y}\right)^2-\beta\rho\omega^2+\frac{\partial}{\partial y}\left[(\mu+\sigma\mu_T)\frac{\partial \omega}{\partial y}\right] \tag{6.29}$$

$$\mu_T=\alpha^*\rho k/\omega,\quad h=C_pT,\quad P=\rho RT \tag{6.30}$$

Viscous effects are unimportant in the defect layer so that the closure coefficients are given by

$$\alpha^*=1,\quad \alpha=5/9,\quad \beta^*=9/100,\quad \beta=3/40,\quad \sigma^*=1/2,\quad \sigma=1/2 \tag{6.31}$$

To analyze the compressible defect layer, we introduce the transformed coordinates ξ and η defined by

$$\xi=x/L,\qquad \eta=\frac{1}{\Delta(x)}\int_0^y\frac{\rho}{\rho_e}\,dy,\qquad \Delta(x)=\frac{U_e\delta_v^*}{u_\tau} \tag{6.32}$$

where U_e and ρ_e are velocity and density at the boundary-layer edge, u_τ is friction velocity, L is a characteristic length scale in the streamwise direction, and δ_v^* is the compressible velocity thickness defined by

$$\delta_v^*=\int_0^\infty\frac{\rho}{\rho_e}\left(1-\frac{U}{U_e}\right)\,dy \tag{6.33}$$

We introduce the streamfunction, $\psi(x,y)$, and its transformed counterpart, $F(\xi,\eta)$, defined by:

$$\psi(x,y)=\rho_eU_e\Delta\,F(\xi,\eta) \tag{6.34}$$

Similarly, we transform the various flow properties according to:

$$\left.\begin{aligned}
u(x,y) &= U_e\mathcal{U}(\xi,\eta);\quad \mathcal{U}=\partial F/\partial\eta\\
\mu_T(x,y) &= \rho_wU_e\delta_v^*N(\xi,\eta)\\
\rho(x,y) &= \rho_eR(\xi,\eta)\\
h(x,y) &= C_pT_eH(\xi,\eta)\\
k(x,y) &= \frac{\rho_w}{\rho}\frac{u_\tau^2}{\sqrt{\beta^*}}K(\xi,\eta)\\
\omega(x,y) &= \frac{u_\tau}{\sqrt{\beta^*}\Delta}W(\xi,\eta)
\end{aligned}\right\} \tag{6.35}$$

The transformed equations of motion possess a similarity solution in which all flow properties are independent of x. The similarity variable is η and the following set of *ordinary differential equations* define the similarity solution.

$$\frac{d}{d\eta}\left[RN\frac{d\mathcal{U}}{d\eta}\right]+\left[\alpha_T-(2-M_e^2)\beta_T-2\omega_T\right]F\frac{d\mathcal{U}}{d\eta}=\beta_TH\left[1-\mathcal{U}^2\right] \tag{6.36}$$

$$\frac{1}{Pr_T}\frac{d}{d\eta}\left[RN\frac{dH}{d\eta}\right] + \left[\alpha_T - (2-M_e^2)\beta_T - 2\omega_T\right] F\frac{dH}{d\eta}$$
$$= (\gamma-1)M_e^2\left(\frac{u_\tau}{U_e}\right)^2 WHK \tag{6.37}$$

$$\sigma^*\frac{d}{d\eta}\left[RN\frac{d}{d\eta}(HK)\right] + \left[\alpha_T - (2-M_e^2)\beta_T - 2\omega_T\right] F\frac{d}{d\eta}(HK)$$
$$= \left[\phi_T - M_e^2\beta_T - 4\omega_T\right] UHK - \frac{\rho_e}{\rho_w}\sqrt{\beta^*}\left[\left(\frac{U_e}{u_\tau}\right)^2 RN\left(\frac{dU}{d\eta}\right)^2 - WHK\right] \tag{6.38}$$

$$\sigma\frac{d}{d\eta}\left[RN\frac{dW}{d\eta}\right] + \left[\alpha_T - (2-M_e^2)\beta_T - 2\omega_T\right] F\frac{dW}{d\eta}$$
$$= \left[\beta_T - \alpha_T + 4\omega_T\right] UW - \frac{\rho_e}{\rho_w}\sqrt{\beta^*}\left[\alpha\left(\frac{U_e}{u_\tau}\right)^2 R^2\left(\frac{dU}{d\eta}\right)^2 - \frac{\beta}{\beta^*}W^2\right] \tag{6.39}$$

and

$$N = \alpha^*\frac{K}{W} \tag{6.40}$$

where M_e is Mach number at the boundary-layer edge and the four parameters α_T, β_T, ω_T and ϕ_T are defined by the following equations.

$$\alpha_T = \frac{2}{c_f}\frac{d\delta_v^*}{dx}, \quad \beta_T = \frac{\delta_v^*}{\tau_w}\frac{dP}{dx}, \quad \omega_T = \frac{\delta_v^*}{c_f u_\tau}\frac{du_\tau}{dx}, \quad \phi_T = \frac{2\delta_v^*}{c_f T_w}\frac{dT_w}{dx} \tag{6.41}$$

A similarity solution exists provided these four parameters are independent of x. Although we have not yet completed our analysis, the remaining steps are straightforward and will be completed during the next year. First, we must introduce asymptotic expansions for the various flow properties. Then, examination of the momentum integral equations should tell us that, similar to the incompressible case, u_τ varies so slowly that the coefficient ω_T is negligible to leading order. For similar reasons, ϕ_T is probably negligible. Further manipulation of the momentum integral equations should yield a relationship between α_T and β_T. The resulting equations should represent the similarity solution with the equilibrium parameter, β_T, as a parameter. The equations can be solved numerically with straightforward modifications to our incompressible defect-layer program.

Chapter 7

Summary and Conclusions

We have made important progress in developing a transition model during the past year. Wilcox[10] presents details of research conducted during the first three months of the project. Briefly, Wilcox[10] describes a low-Reynolds-number version of the $k-\omega$ model and tests it for fully-developed turbulent channel and pipe flow, and for incompressible, transitional flat-plate boundary-layer flow.

In the context of turbulent boundary layers, this report shows that the low-Reynolds-number version of the model retains all of the best features of the baseline, high-Reynolds-number version of the model. Most notably, the model is just as accurate as the baseline model for flows with adverse pressure gradient. This guarantees that the model approaches the correct post-transition, asymptotic state.

In the context of transitional boundary layers, this report shows that, while offering predictions superior to those of simpler correlations designed for use with algebraic turbulence models, more development is needed. Most importantly, transition width is close to measured width only for low transition Reynolds numbers. At higher transition Reynolds numbers, model-predicted transition is much more abrupt than measured.

While an ad hoc change in closure coefficient values clearly improves matters for a Mach 20 case, the change is inconsistent with values required for turbulent boundary layers. The best hope for resolution of the problem lies in the perturbation analysis of Chapter 6. Utilizing the sublayer analysis, we should be able to refine the viscous damping functions to arrive at suitable low-Reynolds-number limiting forms for α^*, α, β^*, and any of the other closure coefficients.

The model's sensitivity to the freestream value of ω, to some extent, mitigates the model's insensitivity to initial profiles. The defect-layer analysis offers promise for quantifying and eliminating this annoying misfeature of the model.

References

1. Wilcox, D. C. "Reassessment of the Scale Determining Equation for Advanced Turbulence Models," *AIAA Journal*, Vol. 26, No. 11, pp. 1299-1310 (1988).

2. Wilcox, D. C., "Turbulence-Model Transition Predictions," *AIAA Journal*, Vol. 13, No. 2, pp. 241-243 (1975).

3. Wilcox, D. C., "Turbulence Model Transition Predictions: Effects of Surface Roughness and Pressure Gradient," AIAA Paper 75-857 (1975).

4. Wilcox, D. C. and Chambers, T. L., "Application of the Turbulence-Model Transition-Prediction Method to Flight Test Vehicles," *Turbulence in Internal Flows*, S. N. B. Murthy, pp. 233-247 (1976).

5. Wilcox, D. C., "A Model for Transitional Flows," AIAA Paper 77-126 (January 1977).

6. Wilcox, D. C., "Alternative to the e^9 Procedure for Predicting Boundary-Layer Transition," *AIAA Journal*, Vol. 19, No. 1, pp. 56-64 (January 1981).

7. Wilcox, D. C. and Marvin, J. G., "Combined Effects of Freestream Turbulence and Mass Addition on Blunt-Body Heating and Transition," Proceedings of the 2^{nd} ASME/JSME Joint Thermal Engineering Conference, Honolulu, Hawaii (March 1987).

8. Mansour, N. N., Kim, J. and Moin, P., "Reynolds Stress and Dissipation Rate Budgets in Turbulent Channel Flow," *Journal of Fluid Mechanics*, Vol. 194, pp. 15-44 (1988).

9. Singer, B. A., Dinavahi, S. P. G. and Iyer, V., "Testing of Transition-Region Models: Test Cases and Data," NASA CR 4371 (May 1991).

10. Wilcox, D. C., "The Remarkable Ability of Turbulence Model Equations to Describe Transition," Fifth Symposium on Numerical and Physical Aspects of Aerodynamic Flows, California State Univ., Long Beach, California (13-15 January 1992).

11. Favre, A., "Equations des Gaz Turbulents Compressibles," *J. Mecan.*, Vol. 4, No. 3, pp. 361-390 (1965).

12. Wieghardt, K. and Tillman, W., "On the Turbulent Friction Layer for Rising Pressure," NACA TM 1314 (1951).

13. Ludweig, H. and Tillman, W., "Investigations of the Wall-Shearing Stress in Turbulent Boundary Layers," NACA TM 1285 (1950).

14. Bradshaw, P., "The Response of a Constant-Pressure Turbulent Boundary Layer to the Sudden Application of an Adverse Pressure Gradient," R. and M. No. 3575, British Aeronautical Research Council (1969).

15. Samuel, A. E. and Joubert, P. N., "A Boundary Layer Developing in an Increasingly Adverse Pressure Gradient," *Journal of Fluid Mechanics*, Vol. 66, p. 481 (1975).

16. Fernholz, H. H. and Finley, P. J., "A Critical Compilation of Compressible Turbulent Boundary Layer Data," AGARDograph No. 223 (1977).

17. Fernholz, H. H., Finley, P. J., Dussauge, J. P. and Smits, A. J., "A Survey of Measuring Techniques in Rapidly Distorted Compressible Turbulent Boundary Layers," AGARDograph No. 315 (1990).

18. Coles, D. E. and Hirst, E. A., *Computation of Turbulent Boundary Layers-1968 AFOSR-IFP-Stanford Conference*, Vol. II, Stanford Univ. (1969).

19. Kline, S. J., Cantwell, B. J. and Lilley, G. M., *1980-81 AFOSR-HTTM-Stanford Conference on Complex Turbulent Flows*, Stanford Univ., CA (1981).

20. Zhang, H. S., So, R. M. C., Speziale, C. G. and Lai, Y. G., "A Near-Wall Two-Equation Model for Compressible Turbulent Flows," AIAA Paper 92-442 (January 1992).

21. Wilcox, D. C., "Application of Low Reynolds Number Two-Equation Turbulence Models to High Reynolds Number Flows," International Conference on Near-Wall Turbulent Flows, Arizona State Univ., Tempe, AZ (March 15-17, 1993).

22. Schubauer, G. B. and Klebanoff, P. S., "Contributions on the Mechanics of Boundary-Layer Transition," NASA TN 3489 (1955).

23. Blair, M. F. and Werle, M. J., "Combined Influence of Free-Stream Turbulence and Favorable Pressure Gradients on Boundary Layer Transition and Heat Transfer," United Technologies Report No. R81-914388-17 (1981).

24. Chen, F.-J., Malik, M. R. and Beckwith, I. E., "Boundary-Layer Transition on a Cone and Flat Plate at Mach 3.5," *AIAA Journal*, Vol. 27, pp. 687-693 (1989).

25. Fisher, D. F. and Dougherty, N. S., "Transition Measurements on a 10° Cone at Mach Numbers from 0.5 to 2.0," NASA TP-1971 (1982).

26. Schubauer, G. B. and Skramstad, H. K., "Laminar-Boundary-Layer Oscillations and Transition on a Flat Plate," NACA Report No. 909 (1948).

27. Blair, M. F., "Influence of Free-Stream Turbulence on Boundary Layer Heat Transfer and Mean Profile Development, Part 1 - Experimental Data," *Transactions of the ASME, Journal of Heat Transfer*, Vol. 105, pp. 33-40 (1983).

28. Swearingen, J. D. and Blackwelder, R. F., "The Growth and Breakdown of Streamwise Vortices in the Presence of a Wall," *Journal of Fluid Mechanics*, Vol. 182, pp. 255-290 (1987).

29. Meier, H. L., Kreplin, H. P. and Ming, X., "Problems Associated with Artificial Boundary Layer Transition," AIAA Paper 83-1673 (1983).

    item Dey, J. and Narasimha, R., "An Integral Method for the Calculation of 2D Transitional Boundary Layers," Report 88 FM 7, Dept. of Aerospace Engineering, Indian Institute of Technology, Bangalore, India (1988).

30. Arnal, D., "Laminar-Turbulent Transition Problems in Supersonic and Hypersonic Flows," AGARD/FDP/VKI Special Course on Aerothermodynamics of Hypersonic Vehicles (1988).

31. Menter, F. R., "Performance of Popular Turbulence Models for Attached and Separated Adverse Pressure Gradient Flows," *AIAA Journal*, Vol. 30, No. 8, pp. 2066-2072 (August 1992).

32. Howard, F., "Thermal Analysis Methods and Basic Heat-Transfer Data for a Turbulent Heating Flight Experiment at Mach 20 (Re-entry F)," NASA TM X-2282 (1971).

33. Wilcox, D. C., *Turbulence Modeling for CFD*, DCW Industries, Inc., La Cañada, CA (1992).

34. Wilcox, D. C., "Dilatation-Dissipation Corrections for Advanced Turbulence Models," *AIAA Journal*, (accepted for publication — to appear 1992).